Investigation of the carbonation mechanism of {CH} and C-S-H in terms of kinetics, microstructure changes and moisture properties

Antoine Morandeau, Mickaël Thiery, Patrick Dangla

Investigation of the carbonation mechanism of CH and C-S-H in terms of kinetics, microstructure changes and moisture properties

A. Morandeau[a,b,*], M. Thiery[a], P. Dangla[b]

[a] *Université Paris-Est, IFSTTAR, MAT, F-75732, Paris, France*
[b] *Université Paris-Est, Laboratoire Navier, Ecole des Ponts ParisTech, IFSTTAR, CNRS, F-77455, Marne-la-Vallée, France*

Abstract

The purpose of this article is to investigate the carbonation mechanism of CH and C-S-H within type-I cement-based materials in terms of kinetics, microstructure changes and water released from hydrates during carbonation. Carbonation tests were performed under accelerated conditions (10% CO_2, 25°C and 65± 5% RH). Carbonation profiles were assessed by destructive and non-destructive methods such as phenolphthalein spray test, thermogravimetric analysis, and mercury intrusion porosimetry (destructive), as well as gamma-ray attenuation (non-destructive). Carbonation penetration was carried out at different ages from 1 to 16 weeks of CO_2 exposure on cement pastes of 0.45 and 0.6 w/c, as well as on mortar specimens ($w/c = 0.50$ and $s/c = 2$). Combining experimental results allowed us to improve the understanding of C-S-H and CH carbonation mechanism. The variation of molar volume of C-S-H during carbonation was identified and a quantification of the amount of water released during CH and C-S-H carbonation was performed.

Keywords: (C) Carbonation, (B) Calcium-Silicate-Hydrate (C-S-H), (B) Microstructure, (D) Portland Cement, (B) Calcium Hydroxide

1. Introduction

Reaction of gaseous CO_2 with calcium-bearing phases in concrete infrastructure components is known to cause a lowering of alkalinity, leading to depassivation and corrosion of rebars. The hydration products which are involved in carbonation are mainly CH[1] and C-S-H. The carbonation mechanism is quite well understood from a physico-chemical point of view according to the CO_2 concentration (especially, in the case of materials made of CEM I cement [1, 2, 3, 4]). Carbonation of CH and C-S-H seems to occur simultaneously [5, 6] although from a thermodynamical point of view carbonation of CH has priority over C-S-H carbonation [7]. The polymorphism of formed $C\overline{C}$ (calcite, vaterite, aragonite, and even amorphous calcium carbonate [8, 9, 10, 11]) has been analyzed according to CO_2 concentration [12, 13, 1, 14] and to the $\frac{C}{S}$ ratio of the initial C-S-H [29] (vaterite, and aragonite in particular, are formed when C-S-H of low $\frac{C}{S}$ is exposed to CO_2). Additionally, Black et *al.* [29] observed amorphous calcium carbonate as the first carbonation products.

The impact of carbonation on the microstructure, as well as on the moisture and transfer properties, is still a subject of research, and even debate. Carbonation may engender important changes of microstructure (porosity, pore size distribution, connectivity, specific surface area, etc.) and moisture properties (carbonation certainly results in water release), and hence significant changes of the transport properties, including water permeability, capillary retention, diffusion of ions and gases (such as CO_2), etc.

It is acknowledged that carbonation leads to a reduction in porosity which is ascribed to the positive difference of molar volume between the hydration products and the formed calcium carbonate $C\overline{C}$. Several previous investigations have highlighted the reduction in porosity after carbonation of CEM I cement-based materials, either on site [15, 16, 17] or under accelerated exposure conditions [18, 19, 20, 21]. This reduction in porosity results in an increase of strength [22, 23, 24, 25].

Nevertheless, it is obvious that the observed decrease in porosity cannot only be due to CH carbonation. As a matter of fact, C-S-H carbonation may significantly contribute to this evolution. C-S-H carbonation has been studied by many authors [13, 26, 27, 28, 29]. All agree on a complex decalcification-polymerisation process of the C-S-H and the formation of amorphous silica gel according to the following reaction:

$$C_xS_yH_z + x\overline{C} \longrightarrow xC\overline{C} + ySH_t + (z - yt)H \qquad (1)$$

The exact stoichiometric coefficients of the previous reaction are not clearly defined. For instance, the amount of water inside the silica gel SH_t is unknown, as well as the exact kind of calcium carbonate which forms (calcite, vaterite or aragonite). That is why, the change in the vol-

*antoinem@princeton.edu

[1] It is recalled that, according to cement notations, C=CaO, H=H_2O, S=SiO_2 and $\overline{C}$=CO_2.

ume of solid phases is unknown and explains the difficulty to quantify with enough accuracy the evolution of porosity induced by C-S-H carbonation. As an illustration, it is possible to imagine that if silica gel becomes very dry (low value of the stoichiometric parameter t in Eq. 1), the amount of released free water increases per mole of formed $\mathrm{C\overline{C}}$ from C-S-H ($z - yt$ goes up). This feature related to the hydration level of SH_t could support the idea of the increase in porosity which has already been observed in the case of cementitious systems made of fly ash or silica fume where pozzolanic C-S-H of low C/S is present [30, 31, 32, 2].

Concerning the influence of carbonation on the pore size distribution of cement-based materials, the limited data which were published in the scientific literature do not show a real consensus. Pihlajavaara [15, 16] was the first to point out that carbonation affects the capillary pores of diameter between 10 and 100 nm by globally reducing their volume in the case of CEM I cement pastes (w/c ranging from 0.3 to 0.6). Matsusato et *al.* [24] observed the same trend on CEM I mortars whose porosity in the range 20-300 nm is reduced by carbonation. In spite of a systematic reduction in total bulk porosity, Houst [33] observed by mercury intrusion porosimetry, carried out on CEM I cement pastes of high water-to-cement ratio ($w/c = 0.8$), a shift of the porosity towards greater pore radii during carbonation. Recently, Miragliotta [20] and Thiery et *al.* [34, 35, 36, 37] came to the same conclusion for low grade CEM I concretes. Bier et *al.* [30] investigated the effect of carbonation on the pore size distribution of cementitious materials which were manufactured with different types of blended cement. It was found that for cement manufactured with a high clinker level, carbonation led to a considerable reduction in the capillary pore volume, whereas, for cement blended with slag, a coarser capillary porosity was formed in the course of carbonation progress. Moreover, it is worth mentioning the studies about the cementation by carbonation of air lime mortars. Studies [10, 38] show an increase of pore volume around 100 nm which is ascribed to the transformation of CH macrocrystals to $\mathrm{C\overline{C}}$ microcrystals. Moreover, the authors generally note a monotonic increase in the volumes of pores with diameters below 30 nm which is attributed to the attachment of $\mathrm{C\overline{C}}$ crystals at the surface of aggregate particles and/or at the surface of CH macrocrystals.

Regarding moisture changes, carbonation of CH releases free water which was originally combined in CH, as it is shown in the following reaction:

$$\mathrm{CH} + \mathrm{\overline{C}} \longrightarrow \mathrm{C\overline{C}} + \mathrm{H} \qquad (2)$$

This supply of water is likely to reduce the space available for the diffusion of CO_2 through the porous network of the cementitious matrix. It can also be involved in moisture transport and in delayed hydration reactions of non-hydrated cement grains. The mentioned supply of water was experimentally observed by Pihlajavaara [15] and Delmi et *al.* [21]. However, as far as the authors of the present article are aware, the amount of released water has never been really quantified and correlated with the degree of carbonation of CH. Furthermore, one can wonder if the stoichiometry in Eq. (2) is respected, *i.e.*, if the mole of water which is produced when one mole of CH is carbonated corresponds to condensate capillary or adsorbed water. What is also essential to know is whether the carbonation reaction of C-S-H is likely to release physical water within the porosity (see Eq. 1) .

The aim of this work is to provide further evidence and improved understanding of the effects of carbonation on the microstructure (porosity and pore size distribution), and moisture properties (liquid-water content) on the basis of mercury intrusion porosimetry and gamma-ray attenuation results. By correlating investigations of the microstructure changes with measurements of the degree of carbonation of the hydration products performed by thermogravimetric analysis, analytical relationships to be implemented in models are proposed to explicitly link the decrease in porosity and the amount of released water to the carbonation level of CH and C-S-H. The article discusses results in the case of CEM I cement pastes and mortars. By working on specimens submitted to ongoing carbonation and by providing carbonation profiles (porosity, amounts of CH and $\mathrm{C\overline{C}}$, moisture content, etc.), the originality of the research is to propose a large number of results in the fields of chemistry and microstructure properties and to correlate them in order to obtain reliable analytical relations representing the behaviour of a CEM I cement-based material exposed to carbonation.

2. Materials

2.1. Formulation and fabrication

An ordinary CEM I cement (CEM I 52,5 N CE PM-ES CP2 NF) was used in order to prepare two cement pastes and a mortar. The Bogue composition is provided in Table 1 by using Bogue's formula. This cement has a low content in C_3A and a high content in C_4AF which is much less reactive than the other clinker phases. As a consequence, we will consider in the following that carbonation of the hydration products resulting from C_3A and C_4AF (mainly AFt and AFm) can be disregarded. The main hydration products able to carbonate are thus CH and C-S-H. The sand used in the mortar is silicious (size 0/4 mm).

[Table 1 about here.]

In order to avoid any early drying, sealed plastic bottles were used as moulds for the preparation of cement pastes and mortars. The plastic bottles were filled in 3 steps and air was removed by vibrating the samples between each step before the bottles were closed. The bottles had been sealed and then put in an anti-segregation rotating system for 24 hours. Finally, a sealed curing was performed for 6 months at 20°C before using the samples for carbonation purpose.

Concerning cement pastes, two different water-to-cement ratio w/c were studied: 0.45 (called CN paste) and 0.6 (called CP paste). The mix-design of the mortar was characterized by $w/c = 0.5$ and $s/c = 2$ (sand-to-cement ratio).

2.2. Pretreatment

After a 6-month sealed curing period, plastic bottles were cut in two pieces in order to obtain two cylinders (height $\simeq$ 60 mm, ϕ =70 mm, as shown in Fig. 1). The samples were preconditioned in order to dry them and allow faster carbonation penetration. To do so, the specimens were first recovered with a self-adhesive aluminium foil over the lateral face and bottom faces, so that all transport phenomena can be considered as unidimensional. Then, the specimens were put for 56 days in an oven controlling temperature at 45°C. Finally, the specimens were kept 56 days in a RH-controlled desiccator at 62± 5% and 20°C by means of a saturated salt solution of NH_4NO_3. The first purpose of such pretreatment was to accelerate the carbonation mechanism by controlling the moisture content of the specimens as close as possible to the optimum RH in the range 40%-70% [39, 40, 18, 35, 4]. The pretreatment also aimed at obtaining a moisture profile in the specimen as uniform as possible. The homogeneity of the moisture profile was controlled by gamma-ray attenuation (see section 6).

[Figure 1 about here.]

2.3. Accelerated carbonation test. Choice of a relevant CO_2 concentration.

Accelerated carbonation was performed using an incubator (Sanyo MCO5-AC) able to control temperature T and CO_2 concentration [CO_2]. The relative humidity was fixed by a saturated salt solution. T and RH, as well as [CO_2], were monitored by using HM70 and GM70 probes (Vaisala), respectively.

Usually, accelerated carbonation tests are performed at CO_2 = 50% in France [41, 42] in order to test carbonation resistance of cementitious matrices in a reasonable limit of time. Nevertheless, some other countries use lower concentration (1 to 10%) fearing that phenomena would be different from natural carbonation. Indeed, a few comparative studies have shown that the chemical composition and the microstructure of cement-based materials carbonated using a high CO_2 concentration was different from that of air-carbonated systems in natural conditions [43, 2, 3]. It has particularly been observed that C-S-H decalcification-polymerisation is more pronounced at high CO_2 concentration, and even that C-S-H can be completely decalcified for $CO_2 > 10\%$ [3]. Note that thermodynamically C-S-H can even decalcify at natural concentration of CO_2 [7]. Moreover, ettringite can still be observed for moderate CO_2 concentration [3] whereas it seem to disappear if $CO_2 > 10\%$ [3, 14]. All the three $C\overline{C}$ polymorphs are generally observed in carbonated samples, *i.e.*, calcite, aragonite, and vaterite, but the formation of aragonite and vaterite seems related to the presence of highly decalcified C-S-H, and hence to a high CO_2 concentration. Since $C\overline{C}$ polymorphs have different molar volume, different variations of porosity according to the carbonation conditions are expected. The difference between air-carbonation and accelerated carbonation conditions is even higher if mineral admixtures are added in the cement [30, 31, 44]. Regarding microstructure aspects, results of the literature suggest that accelerated carbonation at high CO_2 leads to a preferential formation of $C\overline{C}$ crystals on the surface of CH particles, and thereby inhibits further dissolution of this phase [45]. Note that this feature could also be related to the moisture content of the material since the drier the material is, the more the formation of $C\overline{C}$ occurs around the surface of CH crystals due to a lack of liquid-water inside the pores to allow aqueous species mobility [46].

In the present research, a CO_2 concentration of 10% was chosen in order to accelerate the carbonation test in a reasonable limit of time without leading to a dramatically different microstructure, in terms of global porosity at least. As a matter of fact, it has been observed by Thiery et *al.* [36, 37, 47] and by Hyvert et *al.* [14] that 10% CO_2 seems to represent a threshold value below which the porosity evolution related to the formation of $C\overline{C}$ is representative of on-site conditions in the case of CEM I systems. This observation is relevant at a macroscopic-enough level of observation corresponding to global porosity measurements by mercury intrusion for instance. Nonetheless, the CO_2 concentration which would preserve the nanostructure of C-S-H gel (observed by sorption of gases or by NMR for instance) in comparison with natural conditions is probably lower, *i.e.*, around 3% according to Castellote et *al.* [2].

During the carbonation test performed in the present research, the temperature was fixed at 25°C and RH was controlled by means of a saturated salt solution of NH_4NO_3 which is able to fix RH = 62± 5%. The temperature and the CO_2 concentration were kept constant inside the incubator, as shown in Fig. 2. The openings of the carbonation chamber does not seem to disturb too much the CO_2 concentration and temperature since these parameters are rapidly reset to the fixed values after each opening step. However, it is more difficult to maintain RH constant around 62± 5% even if the saturated salt solution of NH_4NO_3 was regularly checked (presence of solid salts). RH shows fluctuations around 59%. In spite of this discrepancy, RH remains close to the optimum RH range 40%-70%.

[Figure 2 about here.]

3. Techniques of carbonation monitoring

Monitoring experiments were performed at different ages from 1 to 16 weeks of exposure of the specimens inside the CO_2 incubator. The purpose is to provide relevant information about the shape of the carbonation front related

to each hydration product, and to assess key parameters related to microstructure changes.

3.1. Phenolphtalein spray test

Phenolphthalein is a pH indicator which is pink-fuchsia if the pH value is above 10 and colourless under 8.3. The specimens dedicated to the phenolphtalein test were split in two half-cylinders. Phenolphthalein was sprayed upon both exposed fresh surfaces. The carbonation depth was determined at each test age in six points along the 6 cm diameter exposed surface (indeed, a measurement is carried out each centimetre by avoiding the edges of the fresh exposed surface). The median result is used to define the carbonation depth X_C (The median is the numerical value separating the higher half of X_C data from the lower half. This statistics parameter is more relevant than the mean value when the data are very dispersed as it is the case generally for X_C).

Fig. 3 shows the time evolution of X_C for both studied cement pastes CN and CP. As expected, CN ($w/c = 0.45$) is more resistant to carbonation than CP ($w/c = 0.60$). A square root of time relation passing through the origin has been used to fit X_C data.

The phenolphthalein spray test is quite easy to use, and allows a fast diagnosis, but it remains a destructive method. It provides only one main information, *i.e.*, the depth which coincides with a given drop of the pH value. Because of the subjective choice of colour and the irregular shape of the front of color change due to the presence of aggregates in the case of concrete, the use of phenolphthalein is likely to imprecise readings. Moreover, this method does not indicate the real shape of the carbonation front. Actually, the CO_2 can have reacted at greater depths than the one indicated by the phenolphthalein test, causing a decrease in the pH beyond the carbonation depth determined by spraying phenolphthalein. $\mathtt{C\overline{C}}$ formation beyond the phenolphthalein-pink border has been demonstrated by means of thermoanalytical methods [48, 49, 6], infrared spectroscopy [50], and gamma-ray attenuation [51, 52, 46]. In addition, the drawback of the phenolphthalein test can be related to the formation of calcite surrounding portlandite crystals, and limiting thus their accessibility and their capacity in buffering the pore solution. Thus, the phenolphthalein color can change from pink to incolor whereas some portlandite is still present. Since phenolphthalein test does not show the real changes which may occur in a partially-carbonated material, depth-profiles are required. These profiles can be provided by gamma-ray attenuation in a non-destructive way, or by thermogravimetric analysis in a destructive way.

[Figure 3 about here.]

3.2. Gamma-ray attenuation method (GRAM)

The Gamma-Ray Attenuation Method (abbreviated here as GRAM) is a non-destructive test able to determine density profiles in building materials. GRAM has commonly been used to quantify porosity and water content profiles within concrete [54, 55, 52]. Moreover, by making reasonable assumptions (no significant water transfer occurs by drying in the short run of an accelerated carbonation test), GRAM can also be used to assess carbonation profiles within concrete by measuring the local density increase due to carbonation (*i.e.*, CO_2 binding) [52].

GRAM is based on the absorption of gamma-rays emitted by a radioactive source of Cesium Cs^{137}. Absorption follows the usual Beer-Lambert law:

$$N = N_I \exp(-\mu\rho l) \tag{3}$$

where N_I represents the number of incident photons in the air and N the number of photons having crossed the sample of thickness l. The density of the material is ρ ($\mathrm{kg.m^{-3}}$). μ ($\mathrm{m^2.kg^{-1}}$) corresponds to the gamma-ray absorption coefficient of the material. Like ρ, the coefficient μ depends on the moisture content and carbonation degree of the material.

The gamma-ray absorption $\mathcal{A}$ is defined as $\ln(N_I/N)$. $\mathcal{A}$ depends on the depth of the specimen which is crossed by the gamma-ray beam, as well as on the time of monitoring (after the drying pretreatment or after a given age of accelerated carbonation). Note that the apparatus used in this study [52, 6] allows a cylindrical specimen to be auscultated at different heights by a robot that moves it vertically through the gamma radiation beam. The specimen is placed in the middle of a tray rotating around its axis. The measurement thus corresponds to the average over a section of material whose height is equal to the diameter of the gamma-ray beam, namely 6 mm.

The variation of absorption $\Delta\mathcal{A}$ between t_C (a date of carbonation) and t_0 (time of the end of pretreatment period) can be inferred from GRAM according to Eq. (4).

$$\Delta\mathcal{A} = \mathcal{A}_0 - \mathcal{A}_C = \ln\left(\frac{N_{I0}}{N_0}\right) - \ln\left(\frac{N_{IC}}{N_C}\right) = (\rho_0\mu_0 - \rho_C\mu_C)l \tag{4}$$

If one considers that there is no significant drying in the course of the carbonation test (the assumption will be checked *a posteriori* in section 4.1), the gamma-ray absorption variation $\Delta\mathcal{A}$ is only tied to CO_2 binding [51, 52, 6]. In this way, the density variation related to carbonation can be assessed according to Eq. (5), as well as the molar content of $\mathtt{C\overline{C}}$ which is formed (per unit volume of porous medium) (see Eq. 6). Moreover, it is perfectly legitimate to consider that there is no additional hydration during GRAM testing in view of the duration of the sealed curing period (6 months, see section 2.1). This assumption will be confirmed in section 5.1.

$$\rho_C - \rho_0 = \frac{\Delta\mathcal{A}}{l\mu_{CO_2}} \tag{5}$$

where $\mu_{CO_2} = 0.0772\ \mathrm{m^2.kg^{-1}}$.

$$n_{CO_2} = n_{\mathtt{C\overline{C}}} = (\rho_C - \rho_0)/M_{CO_2} \tag{6}$$

where M_{CO_2} stands for the molar weight of CO_2. $n_{\overline{CC}}$ is the molar content of formed $\overline{CC}$ (mol.L^{-1} per unit volume of porous material) and n_{CO_2} of bound CO_2 (mol.L^{-1} per unit volume of porous material).

Moreover, GRAM makes it possible to have access to porosity profiles (ϕ) and to liquid-water saturation profile (S) [52, 6]. The assessment of S profiles is provided by performing a GRAM test on a specimen whose distribution of water content is unknown. Gamma-ray absorption $\mathcal{A}$ is monitored at each depth of the specimen. Then, the specimen is saturated under vacuum according to the same protocol as the one used to measure concrete porosity by hydrostatic weighing [56]. Another GRAM test is performed on the saturated sample (the corresponding absorption is denominated by $\mathcal{A}_{sat}$). Finally, the specimen is dried at 105°C until mass stabilization (the measured absorption is denoted $\mathcal{A}_D$). 105°C has been chosen to shorten the period necessary to get porosity profiles. Moreover, the samples are previously saturated under vacuum before being dried at 105°C. Consequently, the shorter is this stage of drying, the less re-hydration of cement grains and dissolution of solid phases (calcium carbonate) are possible after the saturation of the specimens.

The porosity profile can be calculated according to Eq. (7) and the saturation (S) is obtained according to Eq. (8). In the previous equations, ρ_w is the mass density of the liquid-water and $\mu_w = 0.0857$ cm^2.g^{-1} denotes the mass absorption coefficient of liquid-water.

$$\phi = \frac{\mathcal{A}_{sat} - \mathcal{A}_D}{l \rho_w \mu_w} \tag{7}$$

$$S = \frac{\mathcal{A} - \mathcal{A}_D}{\mathcal{A}_{sat} - \mathcal{A}_D} \tag{8}$$

3.3. Mercury intrusion porosimetry (MIP)

MIP was performed with a Micromeritics Autopore IV which determines pore sizes in the range of 3 nm to 500 μm (corresponding to a 0.0035 MPa-400 MPa range of applied pressure). At different times of accelerated carbonation, cylindrical specimens of mortar or cement paste were sawn under water using a wheel saw. Slices of approximately 0.5 cm thick were taken along the length of the specimen.

MIP requires complete removal of water from the sample before mercury intrusion. Moreover, in order to avoid re-hydration of the cementitious system due to the moistening of the samples during the sawing step, the slices have to be dried just after having been sawn. The effect of drying methods (oven-drying under vacuum or not, freeze-drying or organic solvent-water exchange) was investigated in [60, 61, 62]. The results suggest that the freeze-drying method is the less damaging one for the investigation of the pore structure of cement-based materials. As a result, it has been chosen to prepare the samples by freeze-drying.

3.4. Thermogravimetric analysis (TGA)

Thermogravimetric analysis (TGA) is a method used to determine the composition of cementitious materials in terms of CH and $\overline{CC}$ by detecting the sample mass loss during heating from 20°C to 1100°C. The same preparation (freeze-drying) as the one for MIP measurements was used (see section 3.3). Moreover, the samples were ground in a ring roll mill and sieved at 315 μm. TGA experiments were carried out in a dry nitrogen atmosphere with a Netzsch STA 449 F1 Jupiter coupled with a mass spectrometer (MS) Netzsch QMS 403 C Quadrupole.

During TGA, the powder samples were heated at 10°C/min from 20°C up to 1150°C in argon. The mass loss of H_2O related to CH decomposition usually occurs in the range 450-550°C. The escape of CO_2 from $\overline{CC}$ resulting from carbonation can start just after CH decomposition peak (550-600°C) and is generally prolonged until 900-950°C [63]. In the present research, a MS is coupled with the TGA device in order to identify with more accuracy the temperature range related to the emissions of H_2O or CO_2.

The derivative of the mass loss during heating (DTG), coupled here with MS, shows different peaks associated with the emission of H_2O or CO_2. The first peak in the range 20°C-400°C is commonly related to the dehydration of C-S-H, AFm and AFt phases, as well as to the emission of physically-bound water (see Fig. 4). It is very easy to detect the DTG/MS peak related to the dehydration of CH around 450-550°C. Beyond this temperature range, the decarbonation of $\overline{CC}$ is observed with a pronounced emission of CO_2 detected by MS even if residual water can still be emitted between 500 and 700°C. As already illustrated in the literature [64, 65, 46, 66, 47], the decomposition of $\overline{CC}$ is characterized by the presence of three DTG/MS peaks (see Figs. 4 and 5, see section 4.2).

[Figure 4 about here.]

[Figure 5 about here.]

The principle of TGA quantification of CH and $\overline{CC}$ consists in tracing DTG and MS diagrams related to H_2O and CO_2, respectively, finding the beginning and the end of each peak, and measuring the corresponding weight loss which represents a percentage of the mass of the freeze-dried samples. The tangential method is generally used for TGA assessment of CH in order to take into account the C-S-H dehydration in the same temperature range as CH decomposition [85]. However, this technique is less satisfactory for the quantification of $\overline{CC}$, especially if many modes of $\overline{CC}$ decomposition are observed. That is why, a coupled method associating TGA and MS has been used to assess with enough accuracy the amounts of CH and $\overline{CC}$. Thanks to an auto-calibration of MS data, this method is particularly relevant to distinguish the emitted gases, CO_2 or H_2O, when $\overline{CC}$ of low thermal stability (amorphous $\overline{CC}$ for instance) decomposes in the same temperature range as CH.

Furthermore, MIP provides the bulk density of each sample. It makes it possible to express TGA results as amounts of CH or $\overline{\text{CC}}$ per unit volume of the studied material. Considering that $\overline{\text{CC}}$ mainly comes from CH and C-S-H carbonation (see section 2.1), a subtraction with the non-carbonated state allows the determination of the carbonation level of CH and C-S-H according to the following equations:

$$n_{\overline{\text{CC}}}^{\text{CH}} = n_{\text{CH}}^{0} - n_{\text{CH}} \tag{9}$$

$$n_{\overline{\text{CC}}}^{\text{CSH}} = n_{\overline{\text{CC}}} - n_{\overline{\text{CC}}}^{\text{CH}} = n_{\overline{\text{CC}}} - \left(n_{\text{CH}}^{0} - n_{\text{CH}}\right) \tag{10}$$

where n_{CH}^{0}, n_{CH} and $n_{\overline{\text{CC}}}$ represent the CH content in the initial state (noncarbonated) and in the carbonated state, and the content of $\overline{\text{CC}}$ attributed to carbonation. Note that the initial amount of $\overline{\text{CC}}$ present in the noncarbonated sample is subtracted from the assessed amount of $\overline{\text{CC}}$ for a given carbonation state in order to take into account the formation of $\overline{\text{CC}}$ during the preparation of the sample for TGA measurements, as well as the amount of $\overline{\text{CC}}$ which can be initially present in the cement. In Eqs. (9) and (10), $n_{\overline{\text{CC}}}^{\text{CH}}$ and $n_{\overline{\text{CC}}}^{\text{CSH}}$ refer to the molar contents of $\overline{\text{CC}}$ coming from CH and C-S-H carbonation.

3.5. X-day diffraction

X-ray diffraction (XRD) was performed on powder of cement paste (ground and sieved at 80 μm). Data were collected using a PHILIPS PW3830 diffractometer in a $\theta - \theta$ configuration employing CuK$_\alpha$ radiation (λ =1.54 Å with a fixed divergence slit size 0.5°C and a rotating sample stage). The samples were scanned between 4 and 76°C with a scan speed of 0.01°C.s^{-1}.

4. Carbonation mechanism: chemical aspects

4.1. GRAM profiles

Figs. 6 illustrate density profiles from 1 to 16 weeks of carbonation on both cement pastes CN ($w/c = 0.45$) and CP ($w/c = 0.6$). The increase of density $\rho_C - \rho_0$ between the reference state (before exposure to CO_2 or, equally, after the drying pretreatment) and a given age of carbonation is calculated. Note that each profile of density increase is the average of four profiles obtained at the same time of gamma-ray monitoring on different specimens. The error bars take into account uncertainties related to the statistical dispersion (standard deviation) of the four measured profiles at each time of gamma-ray monitoring. In the case of CP, other ages are illustrated until 16 weeks of exposure to CO_2.

The density evolution can be attributed to either CO_2 fixation as solid $\overline{\text{CC}}$, or moisture transfers. In the course of the carbonation test until 16 weeks, it is shown that no significant density variation is detectable from the surface to a given depth (10-15 mm for CN and 25 mm for CP). The fact that the density profile remains stable supports the hypothesis that moisture transfers are not disturbing gamma-ray attenuation measurements and that the increase of density which is monitored is mainly related to CO_2 binding by carbonation. Neither water still in excess in the cement paste after pretreatment, nor water released by carbonation of the hydration products, moves towards outside or inside the sample by drying in the course of the accelerated carbonation test. Note that for ages above 16 weeks, gamma-ray monitoring shows for CP a decrease of density all along the specimen which suggests a non-negligible contribution of transfers of liquid-water released by carbonation from the specimen to the atmosphere (note that spraying phenolphtalein, it has been observed that the specimen was almost fully carbonated). This peculiar behaviour is related to the high w/c of CP which leads to a higher porosity and permeability to liquid-water than CN. The idea assuming that moisture transfers can be neglected in the course of a carbonation test was also made in the case of concrete specimens [52, 6].

In order to validate GRAM measurements, each profile of density increase along the height of the specimen has been integrated (see Eq. 11 where A stands for the cross section of the specimen and h represents its height). This calculation gives access to a GRAM estimation of the mass evolution of the specimen as a whole. This global GRAM assessment is compared to the mass variations of the specimen which have simply been measured with a weighing scale (see Fig. 7-a).

$$\Delta m = A \int_0^h (\rho - \rho_0)(x)\mathrm{d}x \tag{11}$$

Since the first point investigated by the gamma-ray beam is placed 4 mm away from the exposed surface, an assumption has to be made to perform the calculation by integration of the GRAM profile. One considers that the density variation is the same at the specimen surface ($x = 0$) as the value measured at the first point distant of 4 mm from the surface ($x = 4$ mm). A similar assumption is used at the bottom of the specimen ($x = h$). In Figs. 7, a good agreement between GRAM measurements and simple weighing is noticed. It validates the use of GRAM to investigate the local density increase which is related to CO_2 binding onto the cementitious matrix by carbonation.

The analysis of Figs. 6 can be done in the light of two aspects: the penetration depth of carbonation and the maximum amount of CO_2 which can be bound onto the matrix.

This latter is related to the density increase which is measured by GRAM and is observed in the vicinity of the surface where carbonation seems stabilized. The observation of this part of the GRAM curves reflects that CN has a lower degree of carbonation than CP even through CN has a higher initial amount of CH and C-S-H which represent the major amout of carbonatable hydration products (see Tab. 2). From this observation, it can be deduced that the

maximum carbonation level which can be reached within a cementitious matrix depends not only on the content of CH and C-S-H, but also on the accessibility of the hydration products which is certainly lower in CN due to a denser cementitious matrix. Indeed, CH macrocristals contained in CN are embedded in a denser matrix than in CP where CH formation can occur in a more abundant capillary porosity. To go deeper in this analysis, a way to make the difference between the carbonation levels of CH and C-S-H would be necessary in order to investigate the real part of CO_2 which react with both hydration products. TGA-MS has provided a way to do it in this article (see section 4.2).

[Table 2 about here.]

In terms of carbonation penetration depth, the carbonation front is not sharp for both materials CN and CP. This supports the fact that the chemical reactions occurring during carbonation are not instantaneous with respect to CO_2 diffusion through the porous network. This is in agreement with Thiery et *al.* [46].

Carbonation of CP leads to profiles which penetrate deeper than those observed for CN at the same ages of accelerated carbonation. This result is logically related to a higher porosity for CP, and thus a higher CO_2 diffusion coefficient. Furthermore, CP shows a water vapor desorption isotherm which is located below the one of CN [67]. Thus, for the fixed value of relative humidity of 65± 5% imposed during the pretreatment and the accelerated carbonation test, the liquid-water saturation is 0.60 for CN and 0.38 for CP. As a result, it leads to a higher volume of gas in CP than in CN which facilitates CO_2 diffusion.

Fig. 8 illustrates GRAM profiles for the mortars specimens. Unlike cement paste samples (see Figs. 6), the density increase does not seem stabilized in the vicinity of the specimen surface. It shows that a fully-carbonated state has not yet been reached after a 8-week period of exposure to CO_2. Moreover, regardless of these kinetic aspects, it is essential to recall that the CO_2 binding capacity of the mortar remains below the one of the cement pastes (theoretically around 2 times less than CN and CP given the $w/c = 0.5$ and the $s/c = 2$ of the mortar specimen).

[Figure 6 about here.]

[Figure 7 about here.]

[Figure 8 about here.]

4.2. TGA-DTG-MS and XRD characterization

Figs. 9 show diagrams of thermal analysis (TGA and mass spectrometry MS) performed on samples sawn from the surface to the core of a CN specimen after a 8-week period of accelerated carbonation. In this way, the diagrams illustrate results for different levels of carbonation from an almost fully-carbonated state (near the surface) to a non-carbonated state (at the core of the specimen). Fig. 9a represents derivatives of mass loss during heating (DTG).

For the non-carbonated sample (core of the specimen), 4 peaks can be distinguished: C-S-H + calcium sulfate phases (from 100°C to 300°C), $Mg(OH)_2$ (brucite) (around 350-450°C), CH (from 450°C to 550°C) and $C\overline{C}$ (around 750°C). The peak related to $C\overline{C}$ decomposition is very small and the justification of its presence is based either on initial $C\overline{C}$ in cement and mixing water, or on a slight carbonation of CH and C-S-H during the grinding of the samples (315 μm).

As expected, the more the slice is sawn close to the surface exposed to CO_2, the smaller is the peak related to portlandite decomposition. If the degree of carbonation is high (near the surface), three peaks are observed between 500°C and 900°C. The closer the slice is to the surface, the clearer is the differenciation between these 3 peaks. Note that Fig. 9b (MS patterns) makes it possible to confirm that the observed DTG peaks between 500°C and 900°C correspond to an emission of CO_2 related to a decomposition of $C\overline{C}$.

The shape of the DTG diagrams in the temperature range 500°C-900°C is consistent with data from the literature in the case of accelerated conditions of carbonation [12, 8, 5, 68, 46, 69, 4, 47]. Sauman [13] attributes the first peak (750°C-900°C) to the decomposition of calcite. According to the same author, allotropic forms of calcite (vaterite and aragonite) turn into calcite at 500°C during heating. However, these metastable calcium carbonate forms are less stable and decompose in a lower temperature range (650°C-750°C) which corresponds to the second peak of $C\overline{C}$ decomposition observed in DTG and MS diagrams.

Figs. 9 show that the presence of polymorphs of $C\overline{C}$ becomes more significant if the carbonation level is high, which corresponds to the vicinity of the exposed surface. As a matter of fact, many researchs in the field of chemistry of calcium carbonate confirm that the formation of $C\overline{C}$ polymorphs depend on the *p*H of the pore solution. Tai et *al.* [70, 71, 72] show that at 20°C precipitation of calcite is observed if *p*H is above 11 while for lower values vaterite and aragonite form. Moreover, there are researches in the literature which show that metastable phases of $C\overline{C}$ evolve to calcite according to a dissolution-reprecipitation process [73].

DTG diagrams show that a shoulder effect, and even a peak, is observed just behind CH decomposition (500°C-650°C) if the carbonation level is high. MS patterns confirm that CO_2 is emitted in this temperature range (see Fig. 9b). Many authors have pointed out the presence of amorphous $C\overline{C}$ by comparing TGA and XRD data [12, 74, 10]. Stepkowska et *al.* [64, 75] have described the presence of complex compounds of amorphous forms of carbonate hydroxide hydrates (crypto-nano-cristalline forms) whose decomposition happens in such low temperature range. Brecevic [11] indicates that the formation of amorphous $C\overline{C}$ compounds occurs if the *p*H value of the pore solution

is low (below 9) which is certainly the case for our materials when the carbonation level becomes high and for a high CO_2 concentration. According to the same author, amorphous $C\overline{C}$ progressively evolves to calcite according to a dissolution- reprecipitation process, in the same way metastable vaterite and aragonite can evolve to calcite.

It is noteworthy that in a recent study [76] authors have investigated the effect of water vapor and CO_2 on portlandite by Raman Spectroscopy and have shown the presence of amorphous $C\overline{C}$ if $RH < 20\%$, metastable vaterite and aragonite if $20\% < RH < 80\%$ and calcite for higher RH-values.

The DTG diagrams of each slice sawn from the mortar specimen exposed to CO_2 during 8 weeks are shown in Fig. 10. The shape of the DTG diagrams for the carbonated mortar samples are similar to those obtained for CN cement paste. Moreover, one notes the presence of 3 modes of $C\overline{C}$ decomposition. The DTG peak around 900°C, which is observed regardless of the carbonation degree of the sample, can be attributed to the presence of well-crystallized calcite in the sand.

Few data in the scientific literature illustrate the presence of these 3 DTG-MS modes related to $C\overline{C}$ decomposition in the case of natural carbonation. This would mainly be due to the fact that the degree of carbonation is generally not high enough to observe the formation of metastable forms of $C\overline{C}$ and amorphous $C\overline{C}$. Note that Hidalgo et *al.* [44] have verified similar TGA patterns with three peaks above 550°C for naturally-carbonated cement pastes made of CEM I. In the present research, cement paste CN has been exposed to natural carbonation during 6 months in an air-conditioned laboratory at $RH = 55\% \pm 5\%$ and the corresponding DTG diagram is compared in Fig. 11 to the DTG diagrams obtained for CN exposed to 10% CO_2 and for non-carbonated CN. It is obvious that the DTG patterns are similar for both natural and accelerated conditions. Furthermore, XRD diagrams confirm the presence of metastable forms of $C\overline{C}$ (aragonite and vaterite) in samples which were either naturally-carbonated or carbonated under accelerated conditions. Note that polymorphs of $C\overline{C}$ are detected in the non-carbonated sample as well. It may be due to an unavoidable carbonation of the ground powder during XRD measurement.

Concerning the evolution of CH as carbonation progresses, one remarks for CN, CP and the mortar the presence of CH remaining in the vicinity of the specimen surface where an intense carbonation level would be expected and where it has been observed by GRAM that carbonation is stabilized. This phenomenon has already been highlighted in the literature [45, 5, 68]. It would be related to a reduction of accessibility of CH cristals due to the formation of a coating of $C\overline{C}$ which would hinder CH dissolution. This behavior is facilitated if the material has a low water content since in that case the formation of $C\overline{C}$ crystals preferentially occurs near the solid surface.

[Figure 9 about here.]

[Figure 10 about here.]

[Figure 11 about here.]

[Figure 12 about here.]

4.3. Carbonation profiles determined by TGA compared with GRAM profiles

Carbonation profiles are illustrated in Figs. 13 and 14. They correspond to contents of total $C\overline{C}$ or $C\overline{C}$ only related to C-S-H carbonation, and to contents of CH *vs.* depth. They are obtained by TGA-MS (coupled with MIP) according to descriptions provided in section 3.4.

Observing CH content profiles, one notes that there is still a residue of CH on the specimen's edge, regardless of the formulation (CN or CP) and the carbonation time. It seems that this residual portlandite is either non-carbonatable, or its carbonation is drastically slowed down. There are two possible explanations for this behavior:

- It is known that the profile of gaseous CO_2 is not homogeneous in the sample: in fact, the concentration is high (around 10%) for $x = 0$, decreasing to 0% in the vicinity of the carbonation front. Thus, the first few millimetres of the sample are exposed to a high concentration of CO_2, unlike the core of the sample. One can imagine that we observe here the effect of accessibility reduction due to an intense formation of calcite around of CH crystals related to a high CO_2 concentration. Moreover, the low liquid-water saturation degree prevailing in this region due to the drying pretreatment would be responsible to a preferential formation of $C\overline{C}$ directly around CH crystals since the diffusion of ions remains difficult.

- One can mention that the liquid-water saturation degree at the edge of the specimen must be very low in the first 5 mm due to the drying pretreatment, so that the dissolution of CO_2 would be slowed down from a kinetic point of view, and thus the carbonation rate of CH decreased. Note that this explanation would be also responsible for a slowing in C-S-H carbonation kinetics.

Making a decision about these two possible reasons, in fact both related to a slower carbonation rate, is tricky. However, by observing in details the $C\overline{C}$ content profiles for CN and CP (see Figs. 13 and 14), one notes that for CN, $C\overline{C}$ content is higher at the edge (for $t > 4$ weeks), whereas for CP, $C\overline{C}$ content at the edge of the specimen is slightly lower than the slice just behind the surface layer (*i.e.*, $x = 10$ mm) for the three carbonation ages (4, 8 and 16 weeks). Let's remark that these profiles are never obtained on the same specimen since TGA-MS determine carbonation profiles in a destructive way. These observations are leading us to the conslusion that in the CN case the accessibility reduction of CH is mainly responsible for

the residual portlandite at the edge because the C-S-H carbonation continues to produce $\overline{\text{CC}}$. On the contrary, one notes on CP profiles that all the carbonation process is slowed down, including C-S-H carbonation kinetics. The edge of the sample seems in that case too dry to allow normal CO_2 dissolution and this lack of water may be delaying the carbonation reaction.

In Figs. 13 and 14, one notices that C-S-H and CH carbonate simultaneously since there are several points where both carbonation of CH and C-S-H occur. While thermodynamics [77, 78] predict that all CH has to dissolve before C-S-H begin to carbonate, it is confirmed here that the chemical kinetics of dissolution and precipitation must be taken into account if one wants to describe accurately the behavior of CEM I systems submitted to carbonation.

[Figure 13 about here.]

[Figure 14 about here.]

Results obtained from TGA-MS and GRAM can be combined in order to compare these two ways to assess carbonation profiles. Results are presented in Fig. 15 for CN and CP pastes, and in Fig. 17a for the mortar under study. The molar content $n^{\gamma}_{\overline{\text{CC}}}$ is obtained from Eq. (6) for GRAM. It represents the fixed CO_2 upon the cement matrix. TGA-MS and GRAM work well together, with the exception of the edge of the sample for CN where TGA seems to slightly overestimate the amount of fixed CO_2 compared to GRAM. The explanation may rely on the fact that GRAM is not able to investigate the first layer whereas TGA-MS gives access to it.

Another way to compare TGA-MS and GRAM results is to directly represent in a same plot $n^{\gamma}_{\overline{\text{CC}}}$ assessed by GRAM *vs.* $n^{\text{TGA}}_{\overline{\text{CC}}}$ assessed by TGA-MS, as it is illustrated in Fig. 16. It is observed that both methods are consistent. This figure also confirms that TGA-MS leads to an overestimation in the range of high values of $n_{\overline{\text{CC}}}$ corresponding to the edge of the sample. Besides the fact that GRAM is not able to investigate the first millimetres of the specimen, this discrepancy could be explained by the fact that after a long period of accelerated carbonation, our samples have begun to dry and the edge of the sample is likely to suffer a lack of water which is interpreted with GRAM by a decrease of bound CO_2 according to the hypothesis developed in section 6. One will discuss more in details this assumption in section 6.

[Figure 15 about here.]

[Figure 16 about here.]

[Figure 17 about here.]

5. Carbonation mechanism : microstructure aspects

Carbonation leads to big changes in microstructure. Fig. 18a illustrates the differences between a non-carbonated and a carbonated cement paste, in terms of accessible-to-water porosity (obtained by GRAM) and MIP, for both CN and CP. It shows that water accesses a larger range of pores than mercury, thus leading to higher porosity values. The porosity decrease is displayed by both methods of measurement, MIP showing a lower porosity variation ($\Delta\phi_{Hg} < \Delta\phi_w$) (see Fig. 18b). As shown above, CH and C-S-H dissolve simultaneously as CO_2 diffuses through the cement. These changes are leading to a porosity clogging for CEM I cement pastes. One said before that this clogging is partially due to CH carbonation and the fact that the molar volume of the final product ($\overline{\text{CC}}$) is higher than the one of CH, *i.e.* $V_{\overline{\text{CC}}} - V_{\text{CH}} \simeq 35 - 33 = 2$ cm^3.mol^{-1}. But if one wants to have a real description of the microstructural evolution during carbonation, one needs to take into account the C-S-H contribution, as shown in Fig. 18b where it is obviously observed that the majority of the porosity decrease is due to other hydrates than CH carbonation, that is to say here mainly C-S-H. Furthermore, looking at the uncertainities (see Fig. 18b), one can conclude that the order of magnitude is the same for both methods , which means that the C-S-H nanostructure seems relatively unaffected since MIP do not give access to the finest microstructure of the C-S-H. It seems to justify that a 10% CO_2 concentration within the incubator is acceptable (see section 2.3).

5.1. Porosity profiles

In order to illustrate this clogging, it has been plotted porosity profiles obtained by GRAM for both CN and CP in Fig. 19 (see Eq. 7). One reminds here that CO_2 diffuses from left to right in our experiments. A control sample (NC) has been used for CN and for CP in order to check any microstuctural change which would not be due to carbonation. It has been kept under the same temperature and *RH* conditions, as the one in accelerated carbonation, but without CO_2. No significant changes is seen after 16 weeks for the control sample dedicated to CN, neither after 1 year for the control sample corresponding to CP.

The initial porosity can be considered as homogeneous, which means that our fabrication protocol has avoided any segregation of cement particles (see section 2.1). One clearly observes, after 8 and 16 weeks of carbonation (C), a porosity drop along the profile for both CN and CP. Between 8 and 16 weeks, the carbonation front is moving forward through the sample in CN, which is not very surprising. However, one can notice that the edge of the sample for CP suffers a lower decrease in the porosity. It is necessary to link this observation with the previous one made on CP showing a lower carbonation degree for CP at the edge of the sample ($x = 0$) than for $x > 7$ mm (see Fig. 14 and section 4.3).

[Figure 18 about here.]

[Figure 19 about here.]

5.2. Pore size microstructure changes

In Figs. 20, one clearly sees that the pore size distribution (PSD) is significantly affected by carbonation. Fig. 20a presents a clear difference between the non-carbonated (blue curves) and carbonated (black curves) PSD for CN (various samples are illustrated). It is important to notice that all the pores from 1 μm to 4 nm clog up. Fig. 20b shows PSD characterized of partially carbonated materials from NC to C state for the same specimen, sawn at various depths. Various carbonation stages are thus illustrated (slice 0-3 mm is fully carbonated while slice 27-33 mm is non-carbonated). Consequently, the clogging of the whole range of pores accessible to MIP is clearly illustrated.

[Figure 20 about here.]

5.3. Proposals of equations linking chemistry and microstructure changes

If one goes deeper in the investigation, combining MIP, GRAM and TGA allows us to determine the origin of the porosity variation during carbonation. Note that the study will be led at a macroscopic scale in order to identify the links between the changes of the chemical composition of the material related to carbonation (degree of carbonation of each hydration compound, amount of formed calcium carbonate, etc.) and the evolution of global porosity.

If one considers that the porosity variation is only due to CH and C-S-H (here it is reminded that neither AFm nor AFt carbonation are taken into account, due to a low C_3A content in the used cement), this variation can be written as proposed in Eq. (12) where $V_{C\overline{C}}^{CH} = 37$ cm^3.mol^{-1} stands for the molar volume of the calcium carbonate formed by CH carbonation (mainly calcite here, see section 1), and $V_{CH} = 33$ cm^3.mol^{-1} is the CH molar volume.

$$\Delta\phi = \Delta\phi_{CH} + \Delta\phi_{CSH} = n_{C\overline{C}}^{CH}(V_{C\overline{C}}^{CH} - V_{CH}) + \Delta\phi_{CSH} \quad (12)$$

To understand what happens in C-S-H during carbonation, it is needed to develop what lies behind $\Delta\phi_{CSH}$. Eq. (13) shows this variation of porosity related to C-S-H carbonation where $V_{C\overline{C}}^{CSH}$ is the molar volume of the calcium carbonate formed by C-S-H carbonation. $C_xS_1H_z$ is chosen as the stoichiometry of the C-S-H. The formed silica gel corresponds to C-S-H with $\frac{C}{S}$ ratio (C over S molar ratio) equals to zero. It can be considered that the amount of solid silicon is held constant over time, *i.e.*, $n_{CSH}(t_0) = n_{Si}(t_0) \simeq n_{Si}(t)$ from an initially non-carbonated state (t_0) to a given age of carbonation (t). This assumption is mainly based on the fact that the amount of dissolved silica in the pore solution remains negligible in comparison with the solid amount of silicon in C-S-H. In Eq. (13), $V_{CSH}(t_0)$ represents the initial molar volume of C-S-H and $V_{CSH}(t)$ is the C-S-H molar volume corresponding to a given age of carbonation.

$$\Delta\phi_{CSH} = n_{C\overline{C}}^{CSH} V_{C\overline{C}}^{CSH} + n_{CSH}(t_0)(V_{CSH}(t) - V_{CSH}(t_0)) \quad (13)$$

In Fig. 21a, each contribution to the porosity evolution $\Delta\phi$ is illustrated. On one hand, CH dissolution (represented by $-V_{CH}n_{C\overline{C}}^{CH}$, see Eq. 12) and C-S-H decalcification (represented by $n_{CSH}(t_0)(V_{CSH}(t) - V_{CSH}(t_0))$) contribute to open the porosity. On the other hand, calcium carbonate formation related either to CH ($V_{C\overline{C}}^{CH}n_{C\overline{C}}^{CH}$) or to C-S-H ($V_{C\overline{C}}^{CSH}n_{C\overline{C}}^{CSH}$) decreases the porosity. $V_{C\overline{C}}^{CSH}$ is the molar volume of $C\overline{C}$ produced by C-S-H carbonation, chosen here as calcite. The influence of the choice for $V_{C\overline{C}}^{CSH}$ (calcite, vaterite or aragonite) will be studied in Fig. 22b, but we can already say that it remains negligible. Fig. 21b illustrates the sole contribution of porosity variation from C-S-H ($\Delta\phi - \Delta\phi_{CH} = \Delta\phi_{CSH}$ calculated thanks to Eq. 12) as a function of $n_{C\overline{C}}^{CSH}$. This curve clearly shows that C-S-H carbonation is the main contribution to porosity clogging. Nevertheless, $\Delta\phi_{CSH}$ does not appear as an a linear function of $n_{C\overline{C}}^{CSH}$.

[Figure 21 about here.]

An interesting way to evaluate C-S-H carbonation is to calculate the decalcification level of the C-S-H through C/S evolution. For that purpose, the $\frac{C}{S}$ according to Eq. (14) is illustrated. In agreement with [79], the initial ratio is chosen to be $C/S(t_0) = 1.7$ which represents a common value for non-carbonated C-S-H. The initial Ca content in C-S-H $n_{Ca}^{CSH}(t_0) = x \times n_{CSH}(t_0)$ is calculated by means of Powers' theory [81]. Indeed, the degree of hydration of our systems is known (see Table 2) thanks to the CH content used here as a tracer of hydration [82] (it is recalled that 23 g of CH is formed for 100 g of hydrated cement according to Bogue's composition of our cement, see Table 1). Moreover, in the same way, since 75 g of C-S-H is formed for 100 g of hydrated cement, the C-S-H content can be inferred for our studied materials (see Table 2). Then, Eq. (refeq-css-ncsh) provides an expression of the amount of calcium carbonate coming from C-S-H carbonation ($n_{C\overline{C}}^{CSH}$) only as a function of $\frac{C}{S}$. Finally, Eq. (16) allows us to clarify the variation of porosity related to C-S-H carbonation as a function of $n_{C\overline{C}}^{CSH}$ and $\frac{C}{S}$. As previously expected, $\Delta\phi_{CSH}$ is not a linear function of $n_{C\overline{C}}^{CSH}$.

$$\frac{C}{S}(t) = \frac{C}{S}(t_0)\left(1 - \frac{n_{C\overline{C}}^{CSH}}{n_{Ca}^{CSH}(t_0)}\right) \quad (14)$$

$$n_{C\overline{C}}^{CSH} = \frac{C}{S}(t_0)n_{Si}(t_0) - \frac{C}{S}(t)n_{Si}(t) = \left(\frac{C}{S}(t_0) - \frac{C}{S}(t)\right)n_{Si}(t_0) = \left(\frac{C}{S}(t_0 \quad (15)$$

$$\Delta\phi_{CSH} = n_{CSH}(t_0)(V_{CSH}(t) - V_{CSH}(t_0)) = n_{C\overline{C}}^{CSH}\left(V_{C\overline{C}}^{CSH} + \frac{1}{\frac{C}{S}(t_0) - \frac{C}{S}(t)}[V \quad (16)$$

Thanks to Eq. (16), and to the knowledge of $\frac{C}{S}$, $n_{C\overline{C}}^{CSH}$ and $\Delta\phi_{CSH}$ for each point represented in Fig. 21b, the variation of molar volume of C-S-H ($V_{CSH}(t) - V_{CSH}(t_0)$) can be calculated. Results are illustrated in Fig. 22 which is very important in order to dispose of a relevant description of C-S-H behaviour during carbonation, especially for a modelling purpose. In a purely mathematical way, the experimental data are framed by two linear functions (see Fig. 22a). It can be observed that the Y-intercept is between 20 to 40 $cm^3.mol^{-1}$. This value corresponds to the difference between the molar volume of a non-carbonated C-S-H and amorphous silica. If one considers data from literature, a great variability is found for the molar volume of amorphous silica according to Wolery [83]: from 12 to 34 $cm^3.mol^{-1}$. A great variability is also found for the molar volume of C-S-H. For example, Tennis and Jennings [84] give a value between 105 and 126 $cm^3.mol^{-1}$ for a similar C-S-H as the one chosen here ($C_{1.7}S_1H_{1.5}$). These data lead at least to 70 to 114 $cm^3.mol^{-1}$ for the molar volume variation between silica gel and non-carbonated C-S-H which is at least two times higher than the values inferred from Fig. 22a. However, this reading of Fig. 22a by considering very low values of $\frac{C}{S}$ tending to 0 loses its relevance since the minimum value of $\frac{C}{S}$ ratio which has been observed for our cementitious systems exposed to 10% CO_2 is 0.4. Furthermore, the molar volume variation ($V_{CSH}(t) - V_{CSH}(t_0)$) could clearly increase much more than with the linear trend depicted in Fig. 22a for C/S ranging from 0 to 0.4.

In Fig. 22b, the influence of the chosen molar volume for calcium carbonate coming from C-S-H carbonation is studied. One highlights the fact that if $V_{C\overline{C}}$ varies from 34 to 38 $cm^3.mol^{-1}$ (aragonite and vaterite, respectively), the difference in the assessment of ($V_{CSH}(t) - V_{CSH}(t_0)$) is quite negligible compared to the error bars shown in Fig. 22a.

It is essential to keep in mind that the assessment of the $\frac{C}{S}$ provided in case of non-carbonated and fully-carbonated systems is based on a molar balance of calcium and silicon, and not on a Q^1/Q^2 investigation by ^{29}Si Magic Angle Spinning-Nuclear Magnetic Resonance (^{29}Si MAS-NMR) which generally leads to higher values of $\frac{C}{S}$. For instance, Castellote et *al.* [3] obtained 1.79 by a molar balance method instead of 1.87 by ^{29}Si MAS-NMR for a non-carbonated system. Furthermore, the provided assessment of $\frac{C}{S}$ remains global given that decalcified C-S-H (represented by Q^1 and Q^2 peaks in ^{29}Si MAS-NMR diagrams) is not distinguished here from Ca modified silica gel whose $\frac{C}{S}$ can be lower than 0.67 which corresponds to the allowed minimum value for decalcified tobermorite (represented by Q^3 and Q^4 peaks in ^{29}Si MAS-NMR diagrams according to [68]). As a result, this global way to quantify the $\frac{C}{S}$ of our cementitious systems justifies the possibility to get $\frac{C}{S}$ below 0.67. Furthermore, the high heterogeneity of the carbonated cementitious systems studied here (presence of both decalcified C-S-H and silica gel) is in agreement with the fact that the applied CO_2 concentration of 10%, which is quite high, can lead according to Castellote et *al.* [3] to full decalcification of C-S-H and a presence of silica gel.

Finally, it is important to recall the main assumptions which underlie the construction of Fig. 22a:

- Two distinct specimens are used, one to get porosity information by GRAM and another to obtain information by TGA concerning the carbonation degree of CH and C-S-H. The assumption is thus made that the investigation of carbonation progress is repeatable between two different samples, as it has been illustrated in Figs. 6 and 15;
- The amount of C-S-H (stoichiometry $C_xS_1H_z$) is assessed by using a simple hydration model based on Powers' theory which is quite satisfactory for systems made of CEM I after a long time of hydration;
- It has been considered that the carbonatable hydration products are only CH and C-S-H, and that carbonation of aluminate phases remains negligible for the used cement which haves a low C_3A content.

[Figure 22 about here.]

6. Carbonation mechanism: moisture aspects

Using GRAM and Eq. (8) gives us the possibility to know the liquid water saturation (S) and thus water content in our cement paste (see section). One mole of CH releases one mole of H_2O during its carbonation, but we do not really know if C-S-H is loosing physical water or not when it is carbonated. The aim is also to validate the hypothesis which was made before, stating that there is no drying in the course of the carbonation test.

Figs. 23 illustrates the evolution of S by GRAM profiles in time for CN and CP. A control sample has been kept (until 16 weeks for CN and 56 weeks for CP) at the same temperature and RH as the ones put in the CO_2 incubator. Carbonation clearly releases water as seen on the blue and green curves (two different ages of carbonation for CN, 8 and 16 weeks, whereas just 16 weeks is illustrated for CP). It is also observed some drying between 56 and 112 days and between the initial and the final non-carbonated state. This drying could confirm that GRAM can underestimate $C\overline{C}$ content compared to TGA, particularly at the edge of the sample where drying is more important (see section 4.3).

[Figure 23 about here.]

In Fig. 24, the carbonated CH molar content Δn_{CH} is linked to the molar content of water released in the porous media Δn_{H_2O}.

There are four zones in this figure:

- $\Delta n_{H_2O} > \Delta n_{CH}$: given Eqs. (1) and (2), this can only mean that physical water is released by C-S-H carbonation.

- $\Delta n_{H_2O} = \Delta n_{CH}$: the released water comes from CH carbonation.
- $\Delta n_{H_2O} < \Delta n_{CH}$: the released water comes from CH carbonation, but the sample suffers some drying, more important closer to the fourth zone. It can be infered that water is released from C-S-H but drying is too important to observe it.
- $\Delta n_{H_2O} < 0$: drying is so important during our accelerated carbonation tests that there is a lack of water in the sample.

It clearly shows that after 8 weeks, the total amount of physical water released by carbonation is equal to the carbonated amount of CH for CN. After 16 weeks of exposure to CO_2, one tends to observe a lack of water for CN, and a clear drying is affecting CP after such a long duration of carbonation. Nevertheless, these results clearly show that C-S-H do not release physical water during their carbonation. Consequently, in light of these results, C-S-H carbonation, for CEM I cement paste, consists only in decalcification.

[Figure 24 about here.]

7. Conclusion

The purpose of this study was to understand the C-S-H and CH behaviours during carbonation for modelling purpose, in terms of chemical mechanism, microstructural and moisture changes. Experiments were performed by using destructive (phenolphtalein-spray test, MIP, TGA) and non-destructive methods (GRAM) upon two formulations of CEM I cement paste and one mortar. GRAM and TGA results are in good agreement.

TGA was used in order to identify the distribution between $C\overline{C}$ from CH and $C\overline{C}$ from C-S-H. In light of the obtained results, CH and C-S-H carbonate simultaneously. The initial rate of carbonation is quite similar, but while C-S-H are still carbonating, CH carbonation slows down and stops. This is due to the fact that CH becomes less and less accessible for carbonation.

Carbonation effects upon microstructure clearly lead to a porosity reduction. When C-S-H is submitted to CO_2, a decalcification occurs. Calcium ions are released in the porous media, leading to a C-S-H with a molar volume smaller than a non-carbonated C-S-H and to a smaller C/S. As for CH, this volume loss is compensated by $C\overline{C}$ precipitation. Combining TGA and GRAM porosity profile, the presented experiments have allowed to obtain an state equation providing the variation of molar volume of C-S-H according to $\frac{C}{S}$, $\Delta V_{CSH} = f(C/S)$, with a validity range from 0.4 to 1.7 in C/S (see Eq. 17). The definition of $\frac{C}{S}$ is global and represents the calcification level of the mixture of calcium silicate hydrates and Ca modified silica gel.

$$V_{CSH}(t_0) - V_{CSH}(t) = \beta \left(1 - \frac{\frac{C}{S}(t)}{\frac{C}{S}(t_0)} \right) \quad (17)$$

$$0.02 < \beta < 0.04 \quad (\text{L.mol}^{-1})$$

$$\frac{C}{S}(t_0) = 1.7$$

The moisture behavior has also been investigated, confirming that only portlandite releases physical water during carbonation (adsorbed or capillary condensate water) and that C-S-H does not release physical water during carbonation, leading to a highly hydrated silica gel.

No significant drying happens before 56 days of carbonation at CO_2=10% for both studied cement pastes (w/c = 0.45 and 0.6). It validates the hypothesis made at the beginning of our study according to which the density changes related to carbonation are only due to carbon dioxide binding for short carbonation ages.

These results can be summarized with Eqs. (18) and (19):

$$C_{1.7}SH_z + 1.7\overline{C} \longrightarrow SH_z + 1.7C\overline{C} \quad (18)$$

$$CH + \overline{C} \longrightarrow C\overline{C} + H \quad (19)$$

Combining together thermogravimetric analysis, mercury intrusion porosimetry and gammadensitometry to investigate carbonation has provided quantitative information about the mechanism of carbonation. All the obtained results are very important for works about modelling of carbonation, especially if one adds a new difficulty which is the presence of pozzolanic C-S-H.

8. References

References

[1] D. Anstice, C. Page, M. Page, The pore solution phase of carbonated cement pastes, Cement and Concrete Research 35 (2) (2005) 377 – 383.

[2] M. Castellote, C. Andrade, X. Turrillas, J. Campo, G. Cuello, Accelerated carbonation of cement pastes in situ monitored by neutron diffraction, Cement and Concrete Research 38 (2008) 1365–1373.

[3] M. Castellote, L. Fernandez, C. Andrade, C. Alonso, Chemical changes and phase analysis of OPC pastes carbonated at different CO_2 concentrations, Materials and Structures 42 (2009) 515–525.

[4] E. Drouet, Impact de la température sur la carbonatation des matériaux cimentaires - Prise en compte des transferts hydriques, Ph.D. thesis, ENS Cachan (2010).

[5] G. Groves, D. Rodway, I. Richardson, The carbonation of hardened cement pastes, Advances in Cement Research 3 (11) (1990) 117–125.

[6] G. Villain, M. Thiery, G. Platret, Measurement methods of carbonation profiles in concrete : thermogravimetry, chemical analysis and gammadensimetry, Cement and Concrete Research 37 (2007) 1182–1192.

[7] F. Glasser, T. Matschei, Interactions between portland cement and carbon dioxide, in: ICCC, Montreal (Canada), 2007.

[8] R. Kondo, M. Daimon, T. Akiba, Mechanism and kinetics on carbonation of hardened cement, vol. III, in: 5th International Symposium on Cement Chemistry, The Cement Association of Japan, Tokyo, 1969, pp. 402–409.
[9] T. Baird, A. G. Cairns-Smith, D. S. Snell, Morphology and CO_2 uptake in tobermorite gel, Journal of Colloid Interface Science 50 (2) (1975) 387–391.
[10] D. R. Moorehead, Cementation by the carbonation of hydrated lime, Cement and Concrete Research 16 (1986) 700–708.
[11] L. Brecevic, Solubility of amorphous calcium carbonate, Journal of Crystal Growth 98 (1989) 504–510.
[12] W. F. Cole, B. Kroone, Carbon dioxide in hydrated portland cement, ACI Journal 31 (12) (1960) 1275–1295.
[13] Z. Sauman, Carbonation of porous concrete and its main binding components, Cement and Concrete Research 1 (1971) 645–662.
[14] N. Hyvert, A. Sellier, F. Duprat, P. Rougeau, P. Francisco, Dependency of C-S-H carbonation rate on CO_2 pressure to explain transition from accelerated tests to natural carbonation, Cement and Concrete Research 40 (11) (2010) 1582–1589.
[15] S. E. Pihlajavaara, Some results of the effect of carbonation on the porosity and pore size distribution of cement past., Materials and Structures 1 (6) (1968) 521–526.
[16] S. E. Pihlajavaara, E. Pihlman, Effect of carbonation on microstructural properties of cement stone, Cement and Concrete Composite 4 (1974) 149–154.
[17] R. Patel, D. Killoh, L. Parrott, W. Gutteride, Influence of curing at different relative humidities upon compound reactions and porosity in portland cement paste, Materials and Structures 21 (1988) 192–197.
[18] V. Papadakis, C. Vayenas, M. Fardis, Physical and chemical characteristics affecting the durrability of concrete, ACI Materials Journal 8 (1991) 186–196.
[19] V. T. Ngala, C. L. Page, Effects of carbonation on pore structure and diffusional properties of hydrated cement pastes, Cement and Concrete Research 27 (7) (1997) 995–1007.
[20] R. Miragliotta, Modélisation des processus physico-chimiques de la carbonatation des bétons préfabriqués - Prise en compte des effets de parois, Ph.D. thesis, Université de La Rochelle (juin 2000).
[21] M. Delmi, A. Ait-Mokhtar, O. Amiri, Modelling the coupled evolution of hydration and porosity of cement-based materials, Construction and Building Materials 20 (2004) 504–514.
[22] W. Manns, K. Wesche, Variation in strength of mortars made of different cements due to carbonation, in: 5th International Symposium on Cement Chemistry - Vol. III, The Cement Association of Japan, Tokyo, 1968, pp. 385–393.
[23] H. Smolczyk, Written discussion about carbonation evaluation with time on different cements, in: 5th International Symposium on Cement Chemistry, Tokyo (Japan), 1968, pp. 369–384.
[24] H. Matsusato, K. Ogawa, M. Funato, T. Sato, Studies on the carbonation of hydrated cement and its effect on microstructure and strength, in: 9th International Congress on the Chemistry of Cement. Volume 5: Performance and durability of concrete and cement systems, National Council for Cement and Building Materials, New Dehli, 1992, pp. 363–369.
[25] J. Xiao, J. Li, B. Zhu, Z. Fan, Experimental study on strength and ductility of carbonated concrete elements, Construction and Building Materials 16 (2002) 187–192.
[26] Z. Sauman, V. Lach, Long terme carbonation of the phases $3CaO.Al_2O_3.6H_2O$ and $3CaO.Al_2O_3.SiO_2.4H_2O$, Cement and Concrete Research 2 (4) (1972) 453–446.
[27] A. M. Dunster, An investigation of the carbonation of cement paste using trimethylsilylation, Advances in Cement Research 2 (7) (1989) 99–106.
[28] M. Yousuf, A. Mollah, T. R. Hess, Y.-N. Tsai, D. L. Cocke, An ftir and xps investigations of the effects of carbonation on the solidification/stabilization of cement based systems-portland type v with zinc, Cement and Concrete Research 23 (4) (1993) 773 – 784.
[29] L. Black, C. Breen, J. Yarwood, Structural features of *C-S-H* and its carbonation in air - a raman spectroscopic study. Part II: carbonated phases, J. Am. Ceram. Soc. 90 (3) (2007) 908–917.
[30] T. A. Bier, J. Kropp, H. K. Hilsdorf, Carbonation and realcalinisation of concrete and hydrated cement paste, in: J. C. Maso (Ed.), Durability of Construction Materials, Chapman and Hall, London-New York, 1987, pp. 927–934.
[31] T. Bier, J. Kropp, H. Hilsdorf, Formation of silica gel during carbonation of cementitious systems containing slag cements, in: ACI Special Publication SP114-69, ACI, 1989, pp. 1413–1428.
[32] F. Puertas, M. Palacios, T. Vazquez, Carbonation process of alkali-activated slag mortars, J. Mater. Sci. 41 (2006) 3071–3082.
[33] Y. Houst, Diffusion de gaz, carbonatation et retrait de la pâte de ciment durcie, Ph.D. thesis, EPFL, Lausse (Switzerland) (1992).
[34] M. Thiery, G. Villain, G. Platret, Effect of carbonation on density, microstructure and liquid water saturation of concrete, in: D. A. Lange, K. L. Scrivener, J. Marchand (Eds.), Advances in Cement and Concrete, Engineering Conferences International (E.C.I.), Copper Mountain, Colorado, U.S.A., 2003, pp. 481–490.
[35] M. Thiery, Modélisation de la carbonatation atmosphérique des matériaux cimentaires, Ph.D. thesis, Ecole Nationale des Ponts et Chaussées (2005).
[36] M. Thiery, P. Faure, A. Morandeau, G. Platret, J.-F. Bouteloup, P. Belin, Effect of carbonation on the microstructure and moisture properties of cement-based materials, in: V. Freitas (Ed.), XII DBMC (12th International Conference on Building Materials and Components, April 12-15, 2011), Vol. 3, RILEM, Porto (Portugal), 2011, pp. 1–8.
[37] M. Thiery, V. Baroghel-Bouny, A. Morandeau, P. Dangla, Impact of carbonation on the microstructure and transfer properties of cement-based materials, in: Transfert 2012, Ecole Centrale de Lille, 2012, pp. 1–10.
[38] R. Lawrence, T. Mays, S. Rigby, P. Walker, D. D'Ayala, Effects of carbonation on the pore structure of non-hydraulic lime mortars, Cement and Concrete Research 37 (7) (2007) 1059–1069.
[39] G. Verbeck, Carbonation of hydrated portland cement, ASTM Special Publication (205) (1958) 17–36.
[40] H. Wierig, Longtime studies on the carbonation of concrete under normal outdoor exposure, in: RILEM Seminar, RILEM, Hannover, 1984, pp. 239–249.
[41] G. Villain, M. Thiery, Vers un mode opératoire performant et discriminant de carbonatation accélérée des bétons pour ouvrages d'art, Bulletin des Laboratoires des Ponts et Chaussées 267 (1) (2007) 1–18.
[42] XP P18-458: Tests for hardened concrete - Accelerated carbonation test - Measurement of the thickness of carbonated concrete (2008).
[43] M. A. Sanjuan, C. Andrade, M. Cheyrezy, Concrete carbonation tests in natural and accelerated conditions, Advances in Cement Research 15 (4) (2003) 171–180.
[44] A. Hidalgo, C. Domingo, C. Garcia, S. Petit, C. Andrade, C. Alonso, Microstructural changes induced in portland cement-based materials due to natural and supercritical carbonation, Journal of Materials Science 43 (2008) 3101–3111.
[45] J. R. Johnstone, F. P. Glasser, Carbonation of single crystals of portlandite in cement paste, in: 9th ICCCC, vol. 5, New Dehli, 1992, pp. 370–376.
[46] M. Thiery, P. Dangla, G. Villain, G. Platret, Investigation of the carbonation front shape on cementitious materials: effects of the chemical kinetics, Cement and Concrete Research 37 (2007) 1047–1058.
[47] M. Thiery, P. Dangla, P. Belin, G. Habert, N. Roussel, Carbonation kinetics of a bed of recycled concrete aggregates: a laboratory study on model materials, Cement and Concrete Research 46 (2013) 50–65.
[48] A. A. Rahman, F. P. Glasser, Comparative studies of the carbonation of hydrated cements, Advances in Cement Research 2 (6) (1989) 49–54.

[49] Y. F. Houst, F. H. Wittmann, Depth profiles of carbonates formed during natural carbonation, Cement and Concrete Research 32 (12) (2002) 1923–1930.
[50] Y. Lo, H. M. Lee, Curing effects on carbonation of concrete using a phenolphtalein indicator and fourier-transform infrared spectroscopy, Building and Environment 37 (2002) 507–514.
[51] G. Villain, G. Platret, M. Thiery, Two experimental methods to determine carbonation profiles in concrete, ACI Materials Journal 103 (4) (2006) 103–129.
[52] G. Villain, M. Thiery, Gammadensimetry: A method to determine drying and carbonation profiles in concrete, NDT&E International 39 (4) (2006) 328–337.
[53] M. Hamada, Neutralization (carbonation) of concrete and corrosion of reinforcing steel, vol. III, in: 5th International Symposium on Cement Chemistry, The Cement Association of Japan, Tokyo, 1968, pp. 343–369.
[54] E. M. Hussein, T. M. Whynot, A compton scattering method for inspecting concrete structures, Nuclear Instruments and Methods in Physics Research Section A: Accelerators, Spectrometers, Detectors and Associated Equipment 283 (1) (1989) 100–106.
[55] M. C. D. Rocha, L. M. D. Silva, C. Appoloni, O. P. Filho, F. Lopes, F. L. Melquiades, E. A. D. Santos, Moisture profils measurements of concrete samples in vertical water flow by gamma ray transmission method, Radiation Physics and Chemistry 61 (3-6) (2001) 567–569.
[56] NF P 18-459: Concrete - Testing hardened concrete - Testing porosity and density (in French) (March 2010).
[57] J. Olek, S. Diamond, Alteration of polished sections of free lime containing cement clinker by short-term atmospheric exposure, Cement and Concrete Research 21 (5) (1991) 905 – 910.
[58] S. Diamond, Aspects of concrete porosity revisited, Cement and Concrete Research 29 (1999) 1181–1188.
[59] S. Diamond, Mercury porosimetry - An inappropriate method for the measurement of pore size distributions in cement-based materials, Cement and Concrete Research 30 (2000) 1517–1525.
[60] L. Zhang, F. Glasser, Critical examination of drying damage to cement pastes, Advances in Cement Research 12 (2) (2000) 79–88.
[61] C. Gallé, Effect of drying on cement-based materials pore structure as identified by mercury intrusion porosimetry. a comparative study between oven-, vacuum-, and freeze-drying, Cement and Concrete Research 31 (2001) 1467–1477.
[62] G. Ye, The microstructure and permeability of cementitious materials, Ph.D. thesis, Tu Delft (2003).
[63] V. Ramachandran, J. J. Beaudoin, Handbook of thermal analysis of construction materials, Willliam Andrew Publishing, New York, 2002.
[64] E. Stepkowska, J. Blanes, F. Franco, C. Real, J. Perez-Rodriguez, Phase transformation on heating of an aged cement paste, Thermochimica Acta 420 (1-2) (2004) 79–87.
[65] E. Stepkowska, Simultaneous ir/tg study of calcium carbonate in two aged cement pastes, Journal of Thermal Analysis and Calorimetry 84 (2006) 175–180.
[66] I. Galan, F. Glasser, C. Andrade, Calcium carbonate decomposition, Journal of Thermal Analysis and Calorimetry 1–6.
[67] V. Baroghel-Bouny, Water vapour sorption experiments on hardened cementitious materials: Part I: Essential tool for analysis of hygral behaviour and its relation to pore structure, Cement and Concrete Research 37 (3) (2007) 414–437.
[68] G. Groves, A.Brough, I. Richardson, C. Dobson, Progressive changes in the structure of hardened C_3S cement pastes due to carbonation, J. Am. Ceram. Soc. 74 (11) (1991) 2891–2896.
[69] C. A. Garcia-Gonzalez, N. el Grouh, A. Hidalgo, J. Fraile, A. M. Lopez-Periago, C. Andrade, C. Domingo, New insights on the use of supercritical carbon dioxide for the accelerated carbonation of cement pastes, The Journal of Supercritical Fluids 43 (3) (2008) 500 – 509.
[70] C. Y. Tai, P.-C. Chen, Nucleation, agglomeration and crystal morphology of calcium carbonate, AIChE Journal 41 (1) (1995) 68–77.
[71] P.-C. Chen, C. Y. Tai, K. C. Lee, Morphology and growth rate of calcium carbonate crystals in a gas-liquid-solid reactive crystallizer, Chem. Engng. Sci. 52 (21/22) (1997) 4171–4177.
[72] C. Y. Tai, F.-B. Chen, Polymorphism of $CaCO_3$ precipitation in a constant-composition environment, AIChE Journal 44 (8) (1998) 1790–1798.
[73] T. Ogino, T. Suzuki, K. Sawada, The formation and transformation mechanism of calcium carbonate in water, Geochimica et Cosmochimica Acta 51 (1987) 2757–2767.
[74] T. Baird, A. Cairns-Smith, D. Snell, Morphology and CO_2 uptake in tobermorite gel, Journal of Colloid Interface Science 50 (2) (1975) 387–391.
[75] E. Stepkowska, A. Aviles, J. Blanes, J. Perez-Rodriguez, Gradual transformation of $Ca(OH)_2$ into $CaCO_3$ on cement hydration. XRD study XRD study, Journal of Thermal Analysis and Calorimetry 87 (1) (2007) 189–198.
[76] E. Dubina, L. Korat, L. Black, J. Strupi-Suput, J. Plank, Influence of water vapour and carbon dioxide on free lime during storage at 80° C studied by Raman Spectroscopy, Spectrochimica Acta Part A: Molecular and Biomolecular Spectroscopy (2013) –.
[77] D. Kulik, M. Kersten, Aqueous solubility diagrams for cementitious waste stabilization systems: II, end-member stoichiometries of ideal calcium silicate hydrate solid solutions, J. Am. Ceram. Soc. 84 (12) (2001) 3017–3026.
[78] B. Lothenbach, F. Winnefeld, Thermodynamic modelling of the hydration of portland cement, Cement and Concrete Research 36 (2006) 209–226.
[79] J. Chen, J. Thomas, H. F. Taylor, H. Jennings, Solubility and structure of calcium silicate hydrate, Cement and Concrete Research 34 (2004) 1499–1519.
[80] M.-D. Nguyen, M. Thiery, X. Wang, Analyse et modélisation des couplages entre hydratation et dessiccation dans les matériaux cimentaires contenant des cendres volantes, in: AUGC 2009 (27ème Rencontres de l'Association Universitaire de Génie Civil, June 3-5 2009), Université de Rennes, Saint-Malo (France), 2009, pp. 1–10.
[81] T. Hansen, Physical structure of hardened cement paste. A classical approach, Materials and Structures 13 (No.114) (1986) 423–436.
[82] P. Mounanga, A. Khelidj, A. Loukili, V. Baroghel-Bouny, Predicting $Ca(OH)_2$ content and chemcal shrinkage of hydrating cement pastes using analytical approach, Cement and Concrete Research 34 (2004) 255–265.
[83] T. Wolery, Computer program for geochemical aqueous speciation-solubility calculations: Theoretical manual, user's guide, and related documentation, Tech. rep., Lawrence Livermore National Laboratory Report (1992).
[84] P. Tennis, H. Jennings, A model for two type of calcium silicate hydrate in the microstructure of portland cement pastes, Cement and Concrete Research 30 (2000) 855–863.
[85] V. Kocaba, Development and Evaluation of Methods to Follow Microstructural Development of Cementitious Systems Including Slags, Ph.D. thesis, EPFL (2009).

List of Figures

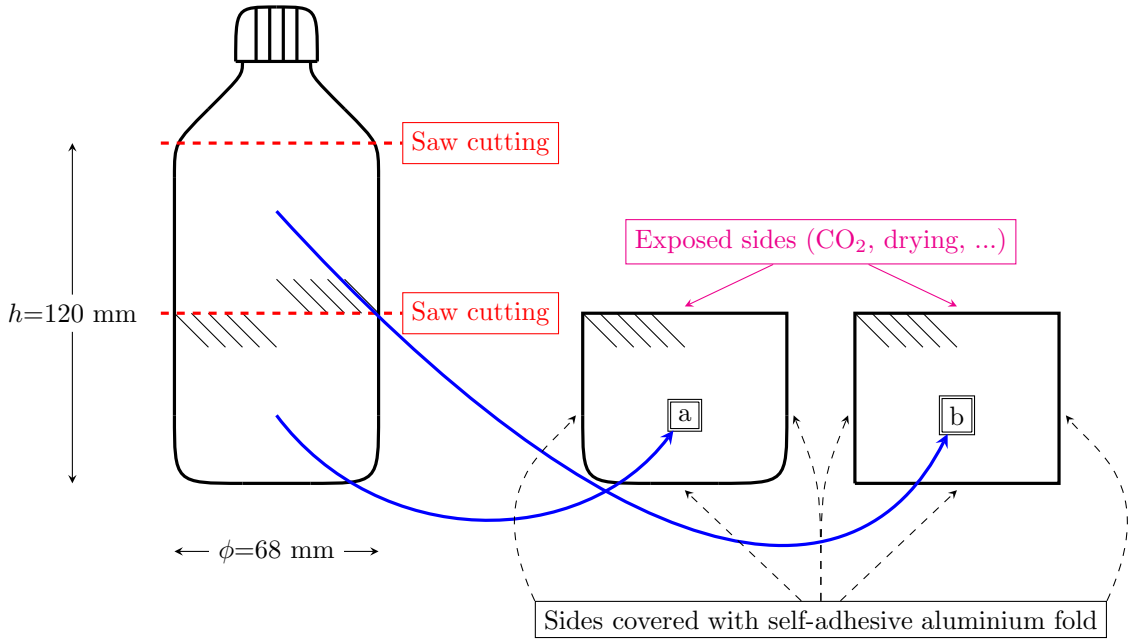

Figure 1: Samples preparation.

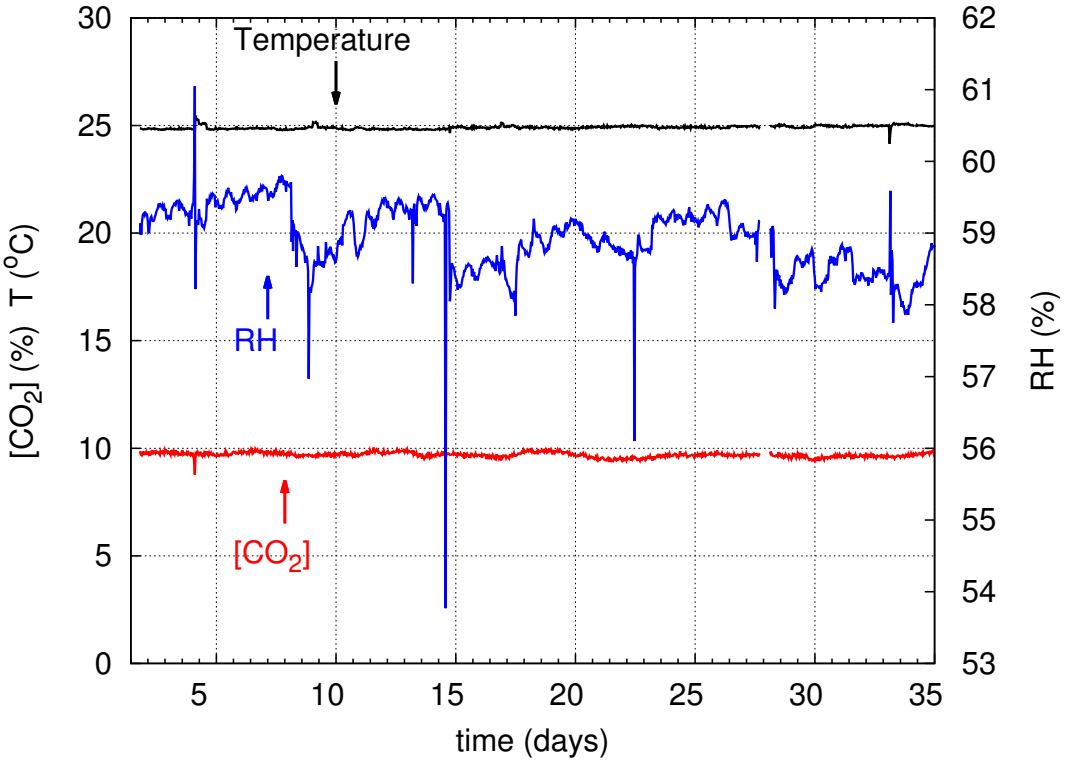

Figure 2: Monitoring example of the environmental parameters (monitoring window of 35 days).

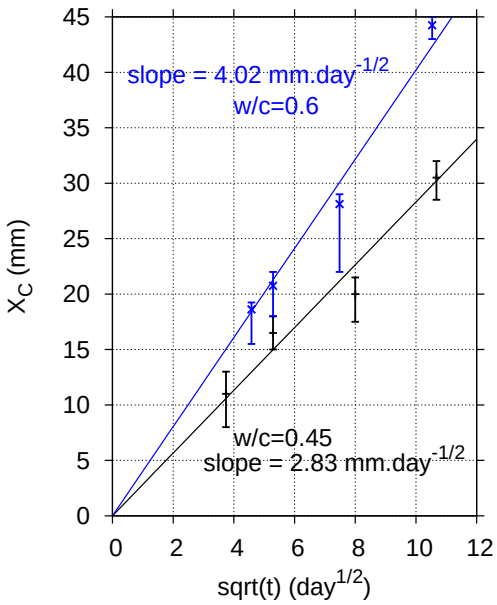

Figure 3: Carbonation depth determined by the phenolphthalein spray test on both CN (w/c=0.45) and CP (w/c=0.6) cement paste after 112 days of carbonation *vs.* square root of time.

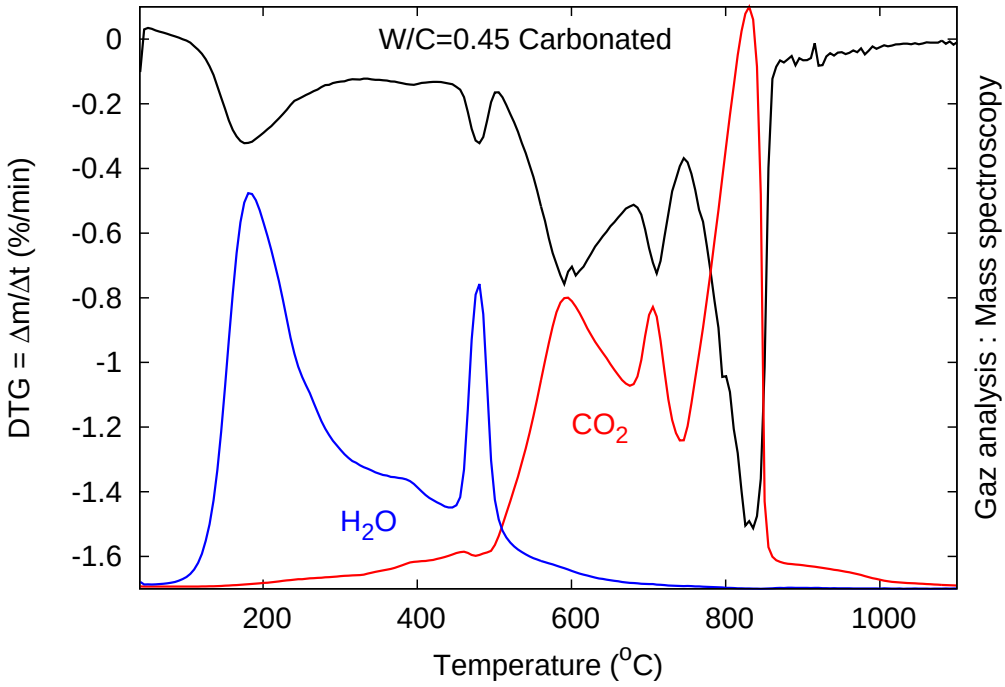

Figure 4: Mass spectrometry (MS) results for a highly carbonated sample of cement paste $w/c = 0.45$. Comparison with the derivative of the mass loss during heating (DTG) peaks.

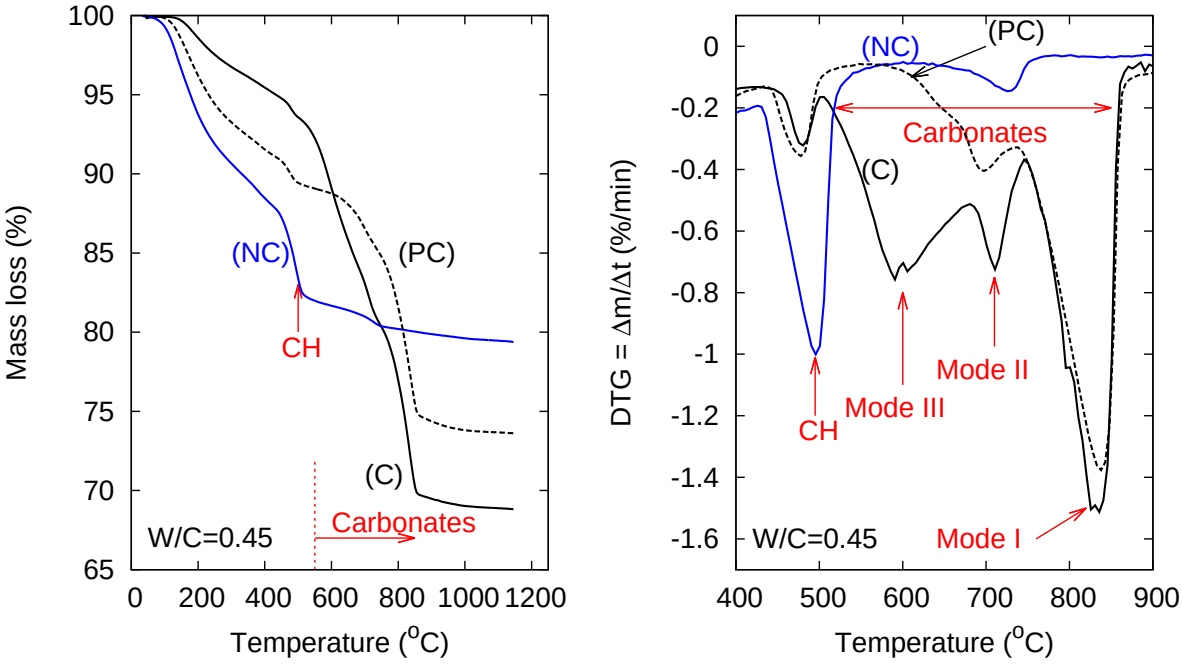

(a) (b)

Figure 5: a/ Mass loss during a TGA experiment on fully carbonated (C), partially carbonated (PC) and non-carbonated (NC) samples (cement paste $w/c = 0.45$). b/ Derivative of the mass loss *vs.* temperature (DTG) in the temperature range corresponding to the decomposition of CH and $C\overline{C}$.

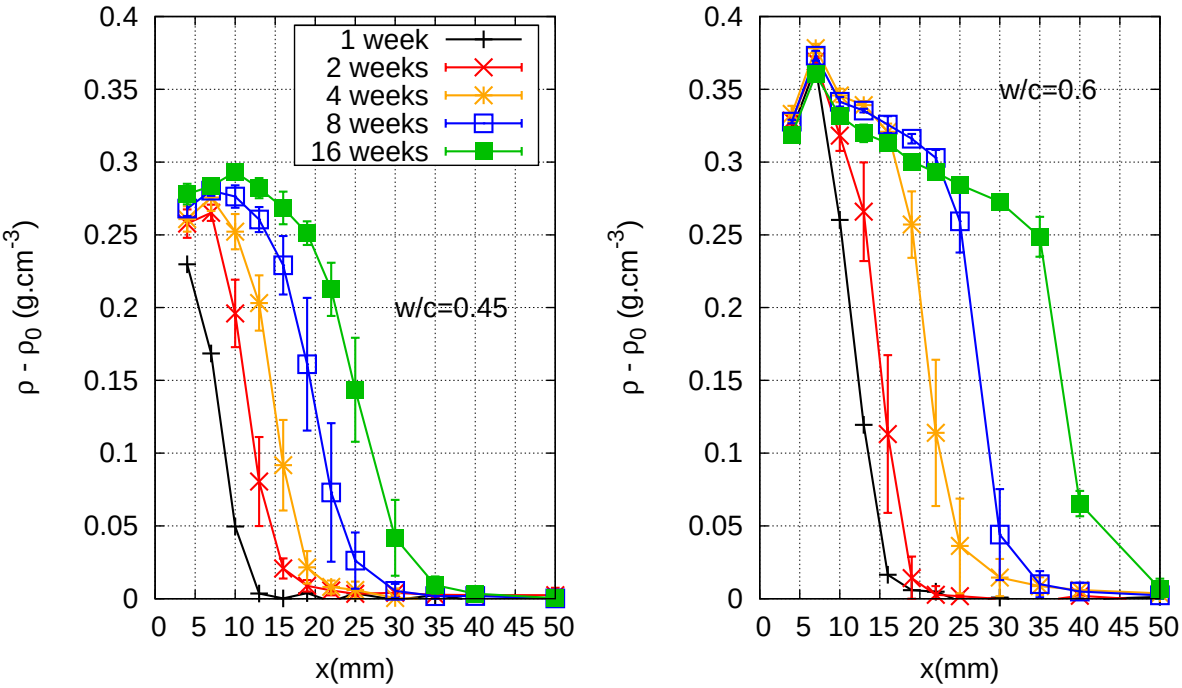

(a) (b)

Figure 6: GRAM profiles on both CN (w/c=0.45, a) and CP (w/c=0.6, b) cement pastes. This figure shows the increase of density measured after 1, 2, 4, 8 and 16 weeks of exposure inside the incubator.

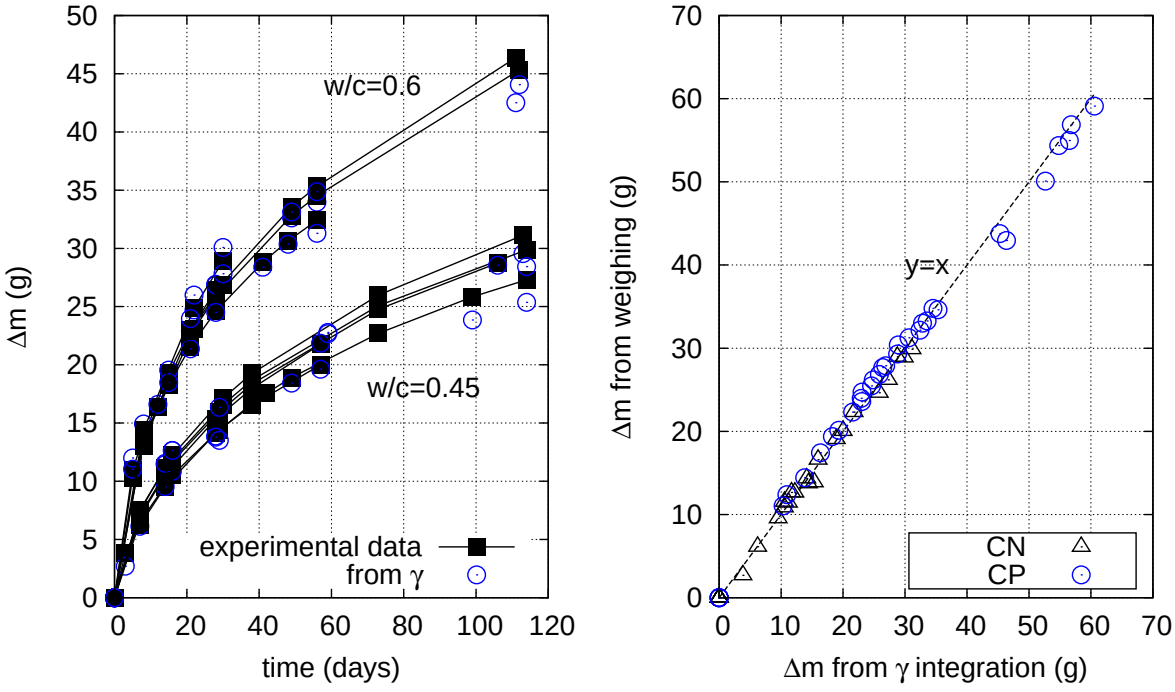

(a) (b)

Figure 7: Two ways to assess the variation of the global mass of the specimen: integration of GRAM profiles and simple weighing of the mass gain from GRAM. Fig. (a) shows Δm from both methods and GRAM profile integration *vs.* time while Fig. (b) shows that both methods perfectly match in a $y = x$ representation.

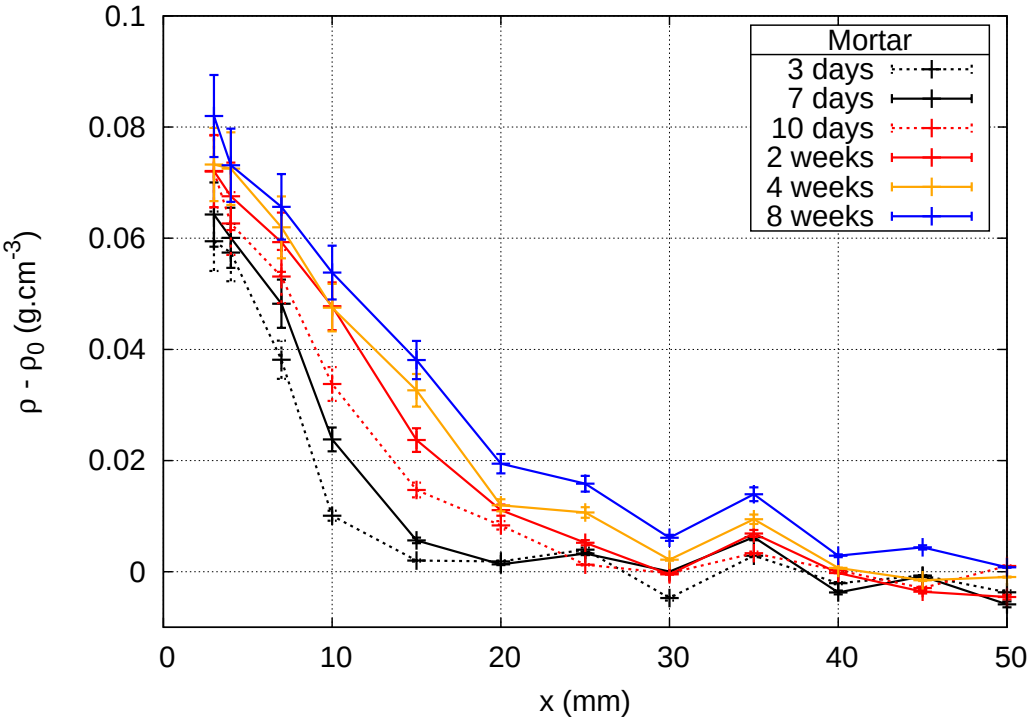

Figure 8: GRAM profiles for the mortar specimen ($w/c = 0.50$ and $s/c = 2$).

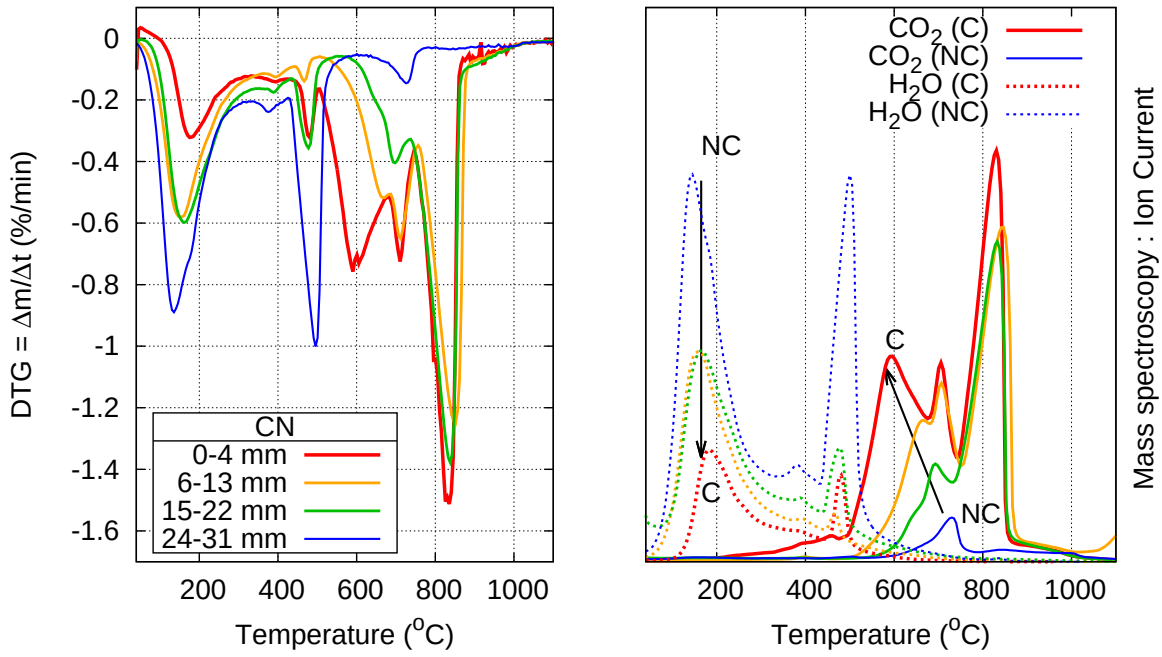

(a) (b)

Figure 9: Diagrams of thermal analysis of samples sawn from the surface exposed to CO_2 to the core of a CN specimen exposed to 10% CO_2 during 8 weeks. (a) DTG diagrams and (b) mass spectroscopy diagrams.

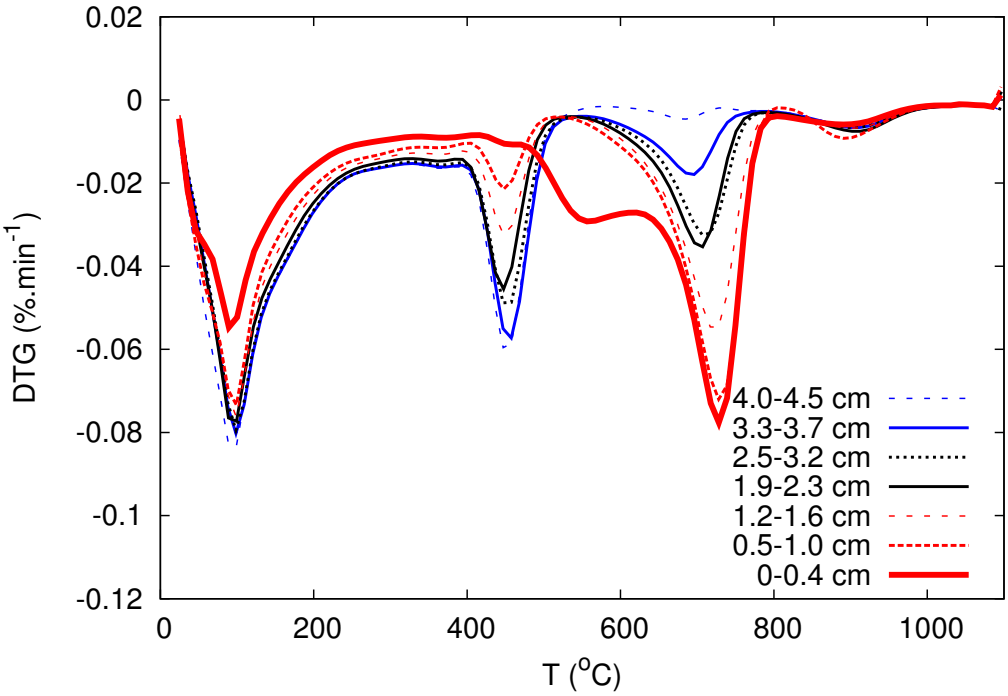

Figure 10: DTG diagrams of the slices sawn from the mortar specimen exposed to 10% CO_2 during 6 weeks.

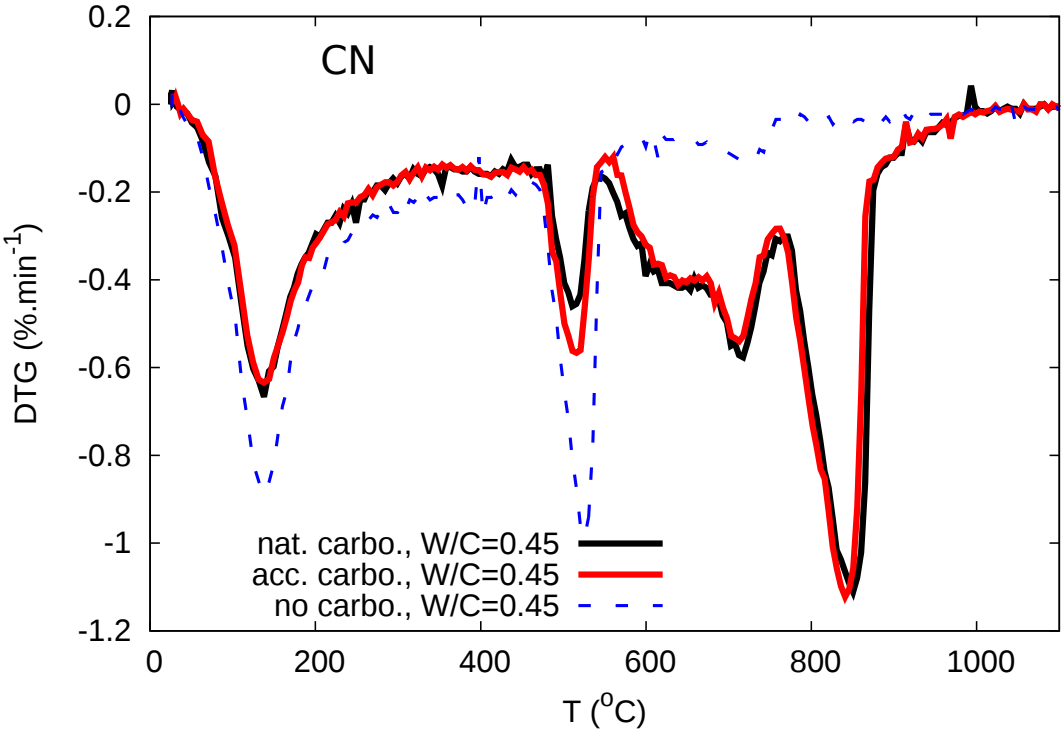

Figure 11: Comparison of DTG diagrams between non-carbonated and carbonated CN (10% CO_2 or natural carbonation).

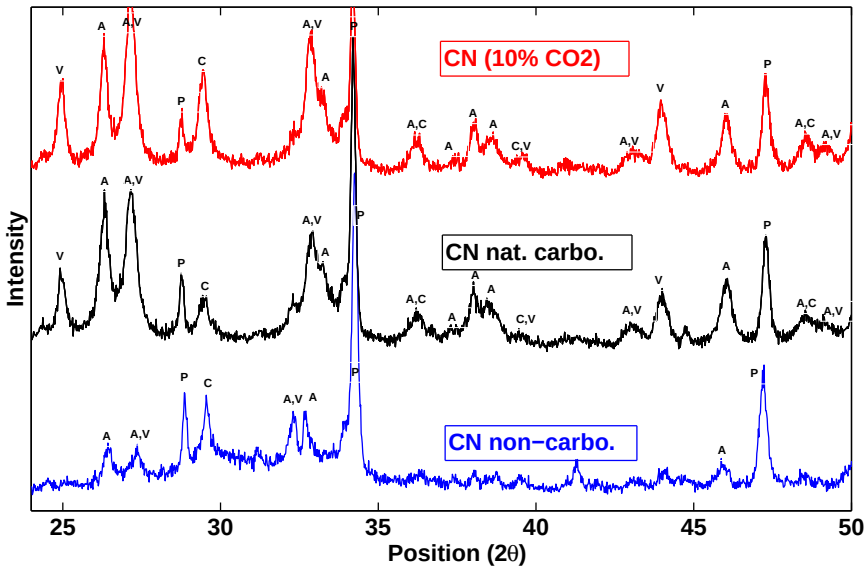

Figure 12: Comparison of XRD patterns for non-carbonated and carbonated (natural conditions and CO_2=10%) CN samples. A for aragonite, V for vaterite, C for calcite and P for portlandite.

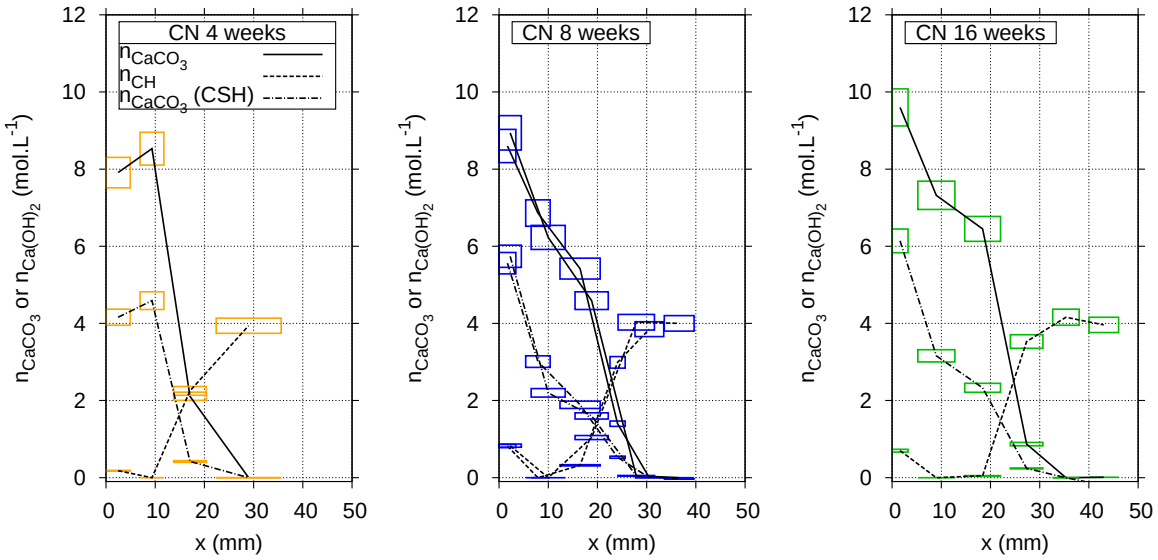

Figure 13: Carbonation profiles assessed by TGA-MS. Illustration of contents of `CH` and $\overline{\texttt{CC}}$ (for $\overline{\texttt{CC}}$, total content and content only related to `C-S-H` carbonation are illustrated) after 4, 8 et 16 weeks of exposure to CO_2. Case of CN paste. For the case of 8 weeks of exposure, the profiles for two different specimens are shown.

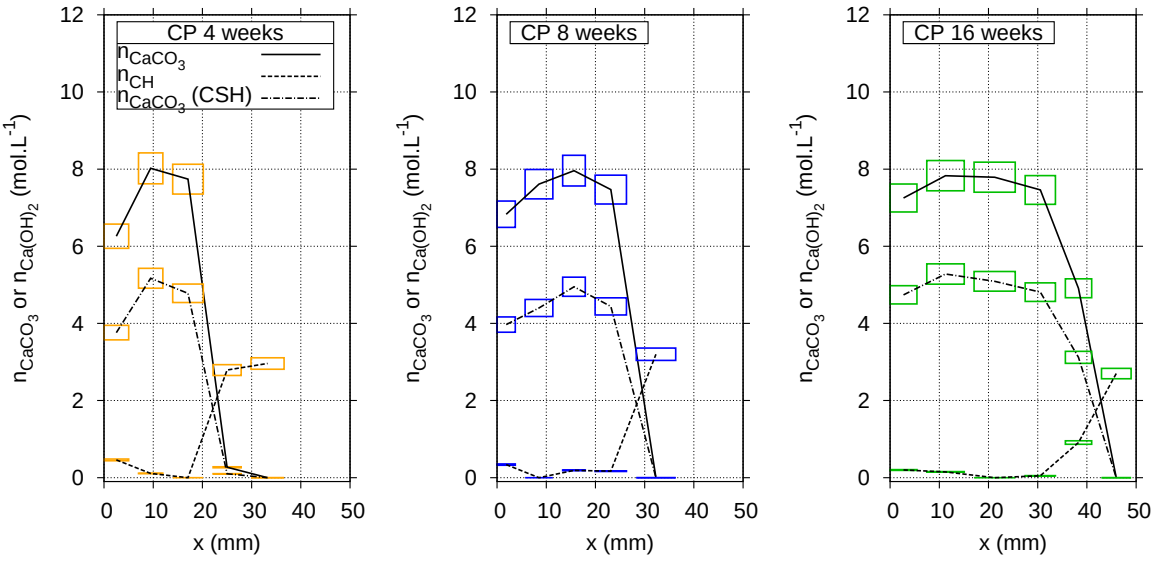

Figure 14: Carbonation profiles assessed by TGA-MS. Illustration of contents of CH and $\overline{\text{CC}}$ (for $\overline{\text{CC}}$, total content and content only related to C-S-H carbonation are illustrated) after 4, 8 et 16 weeks of exposure to CO_2. Case of CP paste.

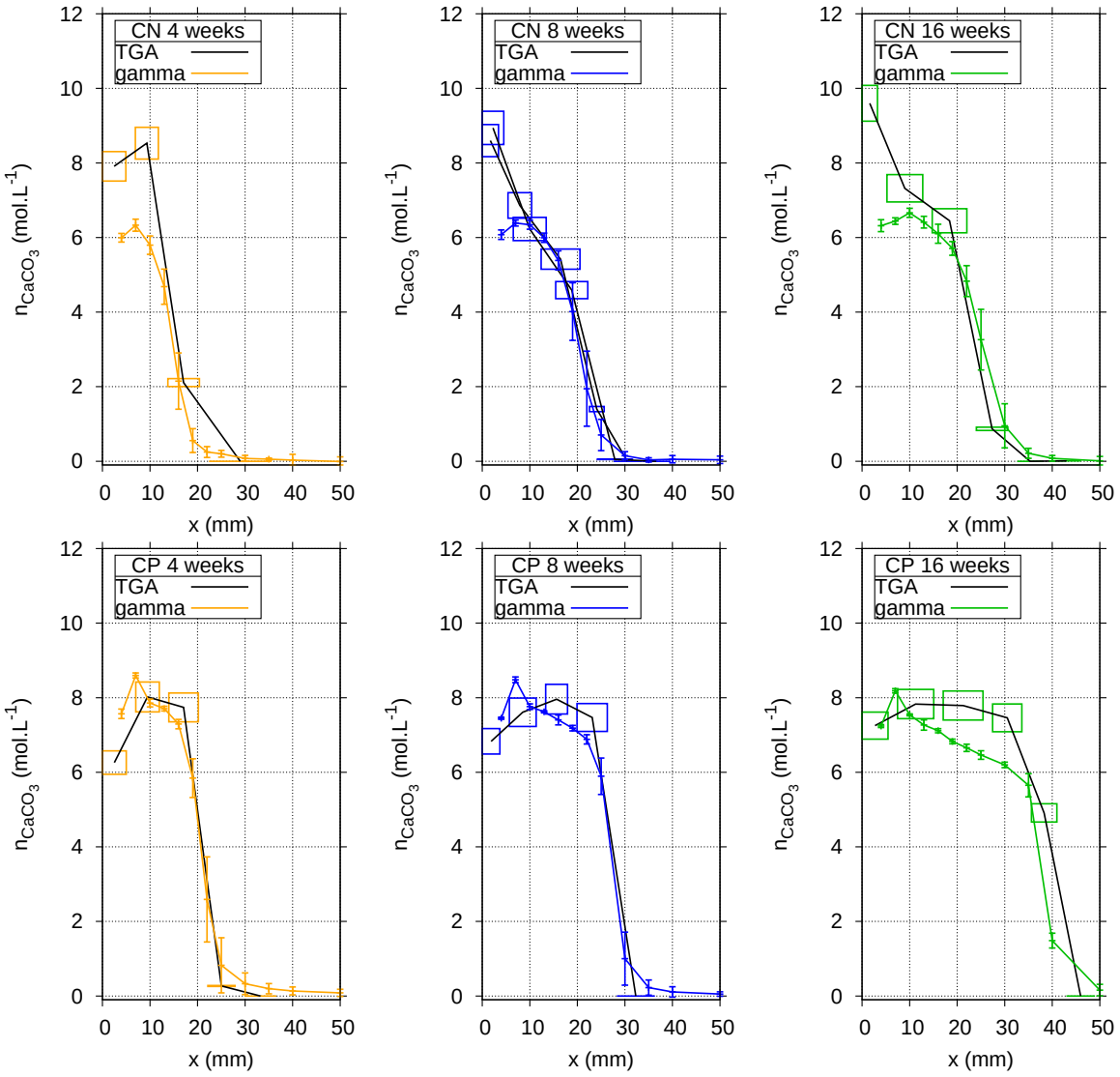

Figure 15: Assessment of CO_2 fixed to the cement matrix as $\overline{\text{CC}}$ ($n_{\overline{\text{CC}}}$) for CN and CP after 4 (orange), 8 (blue) and 16 (green) weeks of accelerated carbonation. TGA-MS data are represented by coloured boxes while GRAM data are represented as coloured lines.

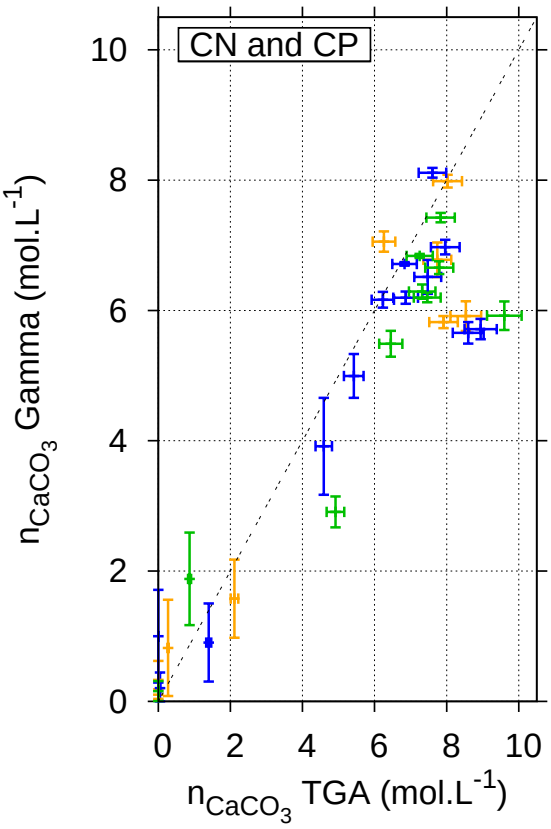

Figure 16: Comparison between $n_{c\overline{c}}$ obtained by TGA-MS and by GRAM.

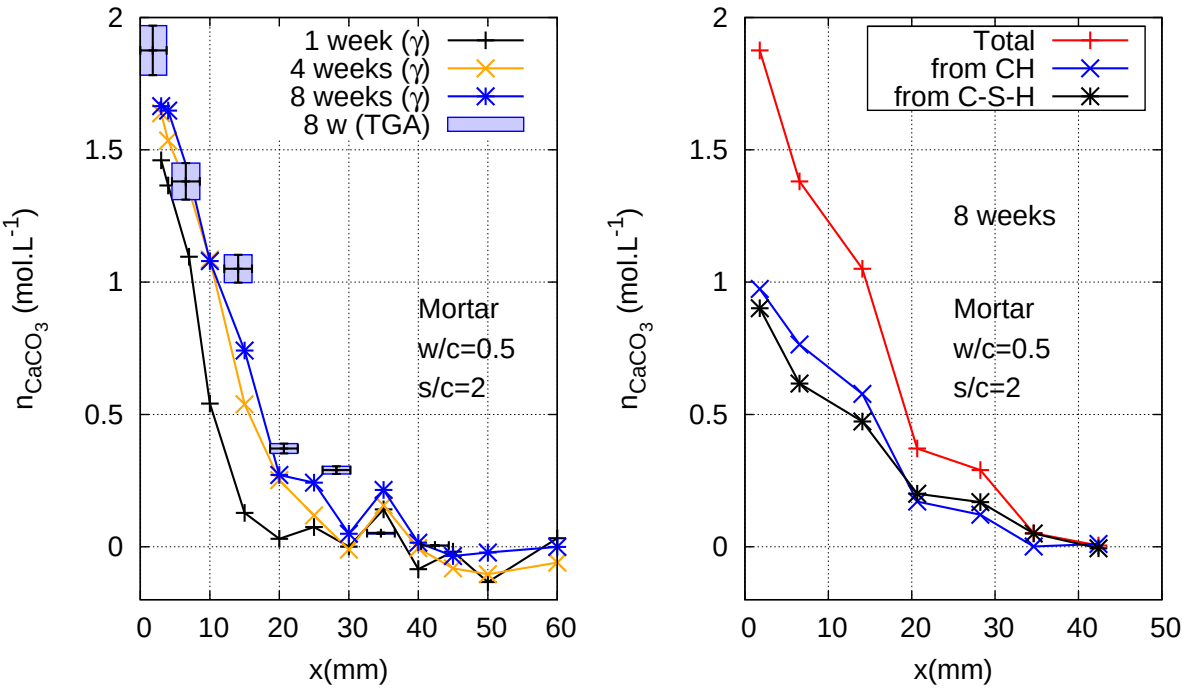

(a) (b)

Figure 17: (a) Content of the CO_2 fixed to the cement matrix as $\overline{\mathtt{CC}}$ are represented for the studied mortar (CEM I cement, w/c=0.5 and s/c=2). TGA results are represented by coloured boxes while GRAM are represented as coloured lines. (b) Quantification of total $\overline{\mathtt{CC}}$ (red) and balance between $n^{\mathtt{CH}}_{\overline{\mathtt{CC}}}$ (blue) or $n^{\mathtt{CSH}}_{\overline{\mathtt{CC}}}$ (black) after 8 weeks of carbonation for the mortar

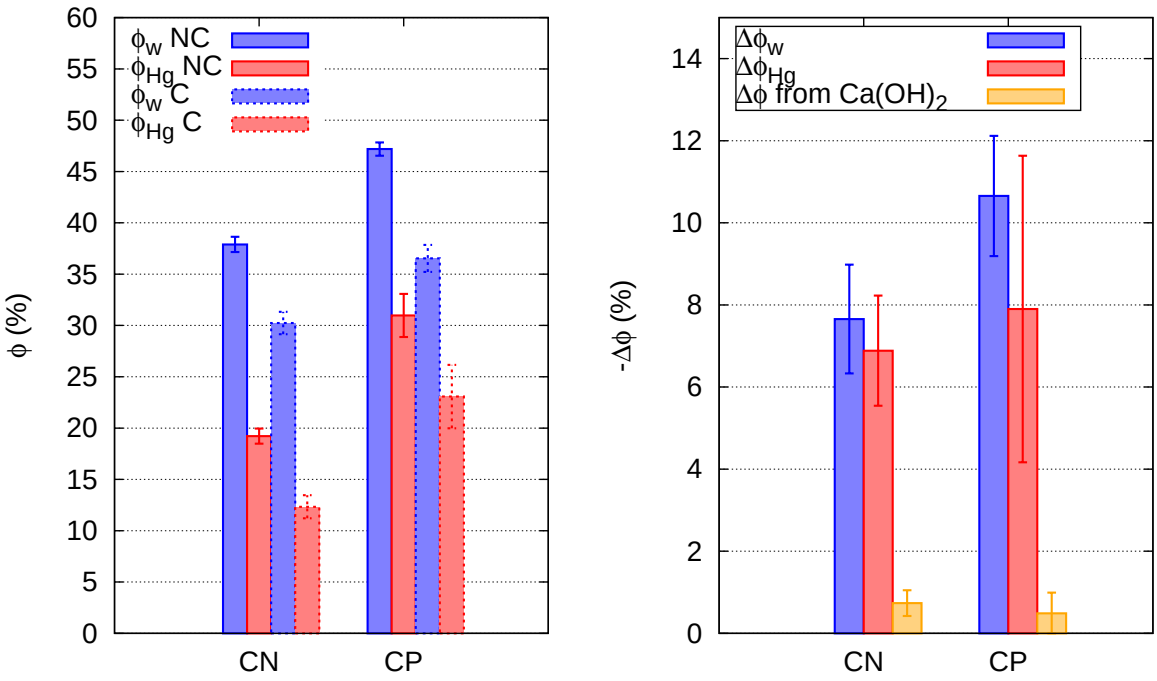

Figure 18: Fig. (a) represents total porosity measured by MIP ϕ_{Hg}, total porosity measured by GRAM ϕ_w, for carbonated (C) and non-carbonated (NC) cement pastes is presented. Fig. (b) represents the variation of porosity between a non-carbonated state and a totally carbonated state for both MIP and GRAM. While the porosity is different, the porosity variation is equivalent. It is also presented the porosity variation only due to CH carbonation (see Eq. 12).

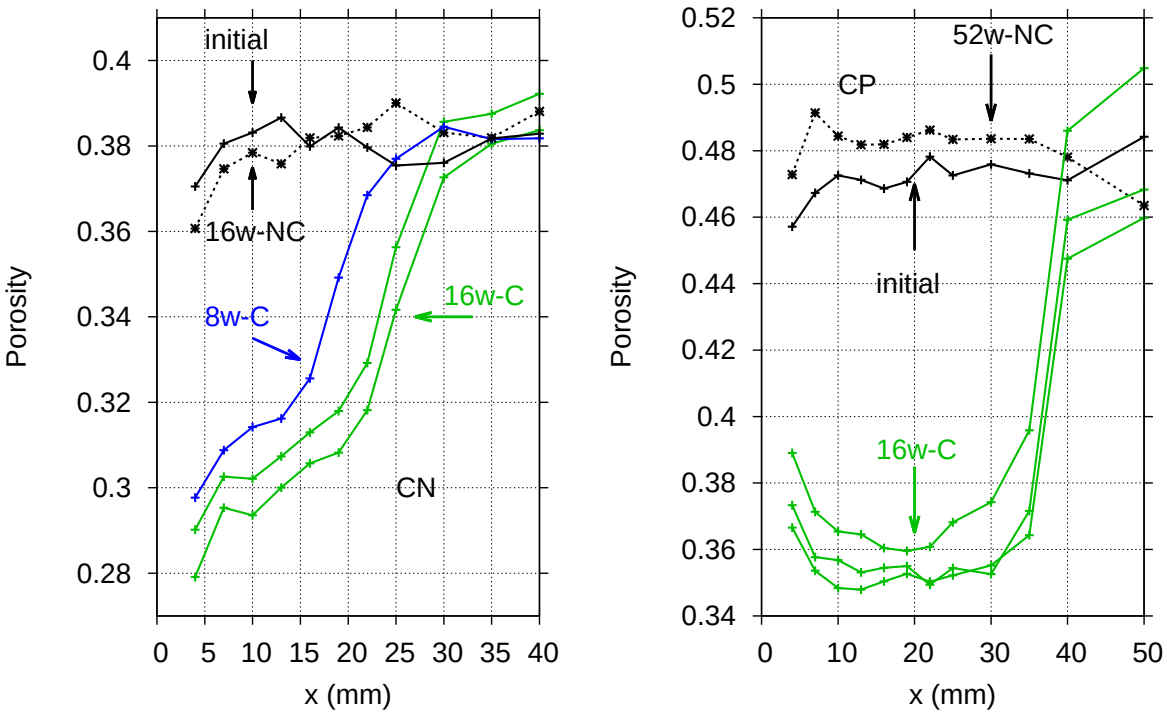

(a) (b)

Figure 19: Porosity profile for both CN (a) and CP (b) at the initial state, after 56 and 112 days of carbonation (56d-C and 112d-C, resp), and after 112 days of drying (112d-NC).

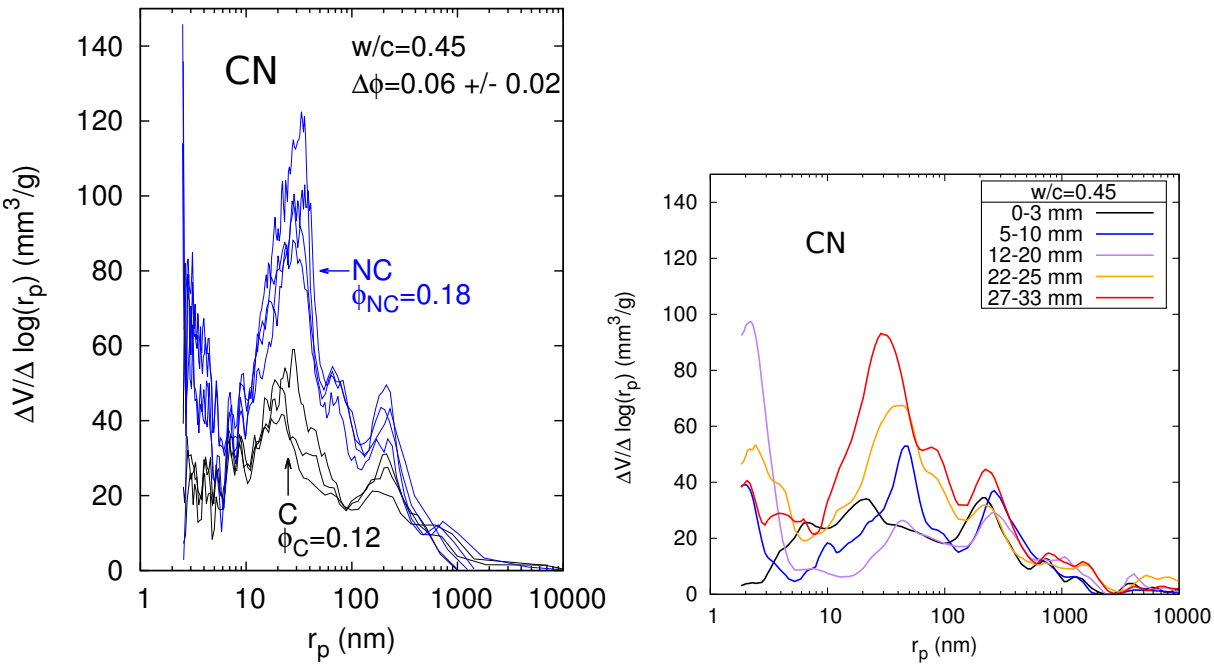

(a) (b)

Figure 20: In Fig. (a), MIP allows us to characterize the pore size distribution in carbonated (C) and in non-carbonated (NC) samples for CN. The variability of the results is presented for various specimen. The PSD is plotted in Fig. (b) for one specimen saw at various depths which represents different carbonation stages.

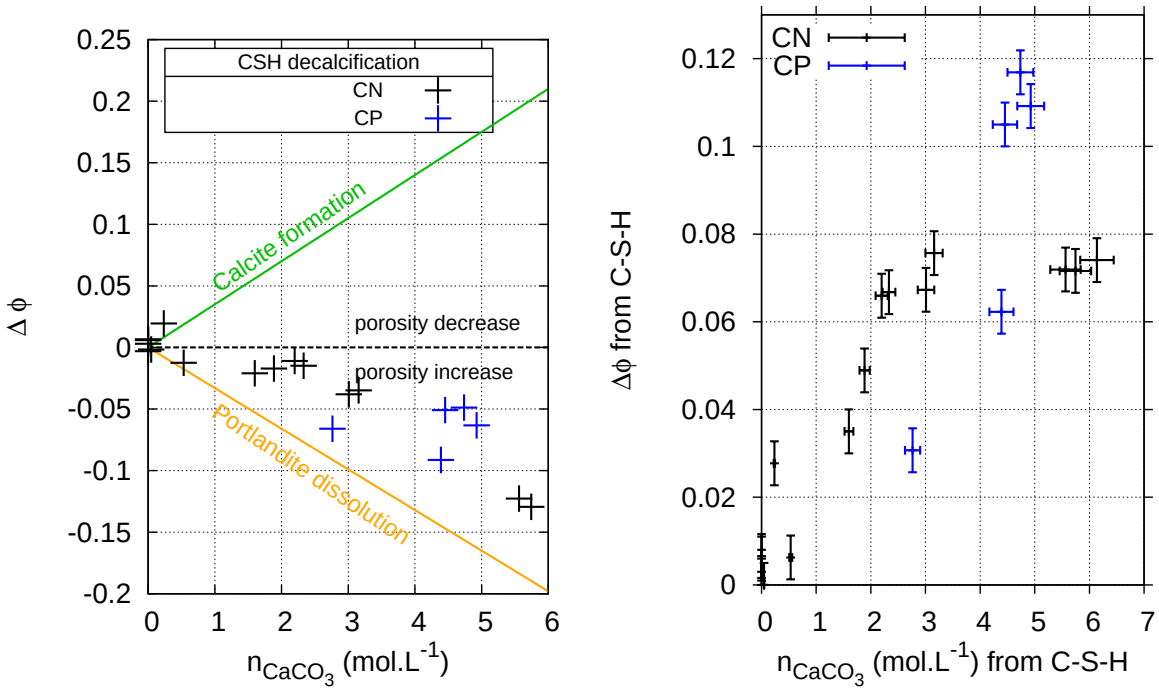

(a) (b)

Figure 21: Fig. (a) shows each contribution for each chemical: mechanism, mainly calcium carbonate formation (chosen here as calcite), CH dissolution and C-S-H decalcification. In Fig. (b), the porosity variation for C-S-H is illustrated as a function of calcium carbonate coming from C-S-H decalcification.

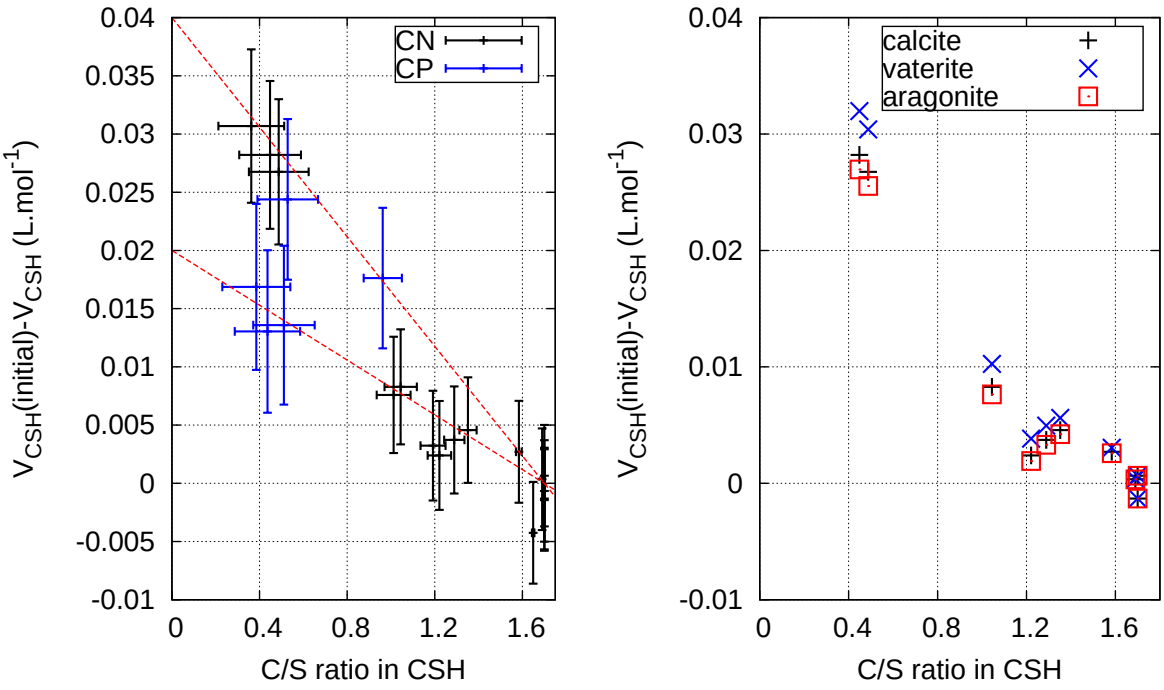

(a) (b)

Figure 22: (a) C-S-H molar volume variation as a function of C/S for both CN and CP. (b) influence of the choice of $V_{C\overline{C}}^{CSH}$, results obtained for various polymorphic forms of $C\overline{C}$ from C-S-H plotted only for CN.

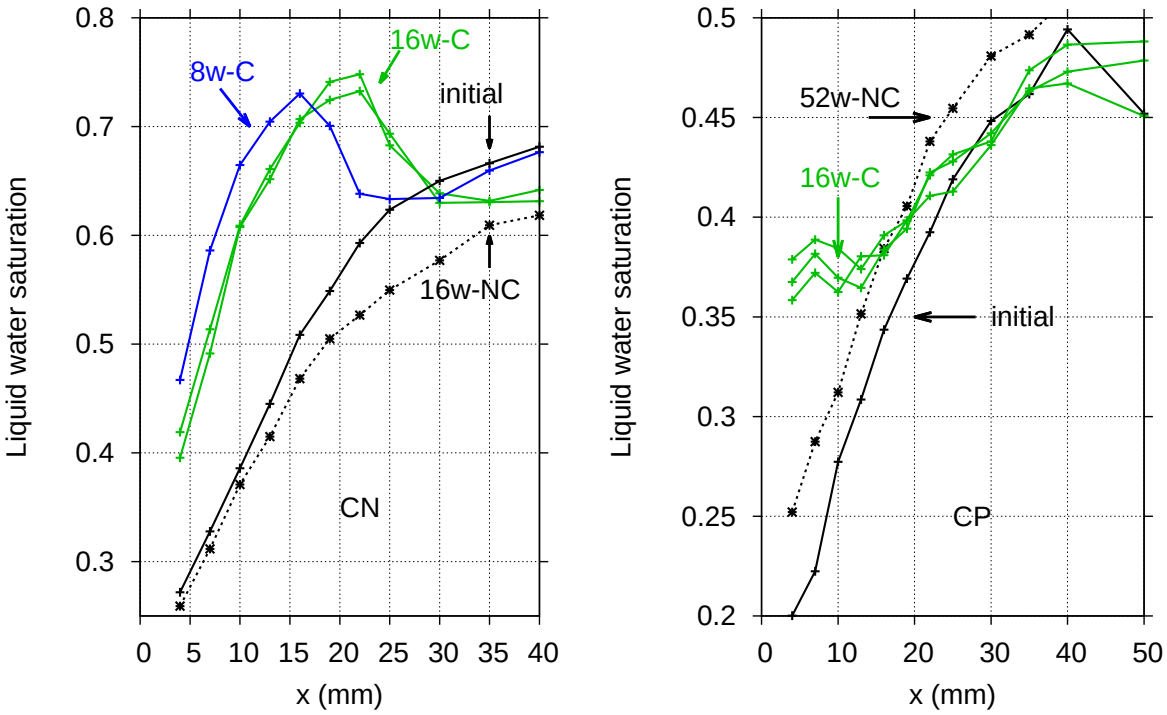

(a) (b)

Figure 23: Water saturation profile obtained by GRAM for both CN and CP at the initial state, after 8 and 16 weeks of carbonation (8w-C and 16w-C, resp.). The profiles for the control specimens are illustrated (16 weeks for CN and 52 weeks for CP).

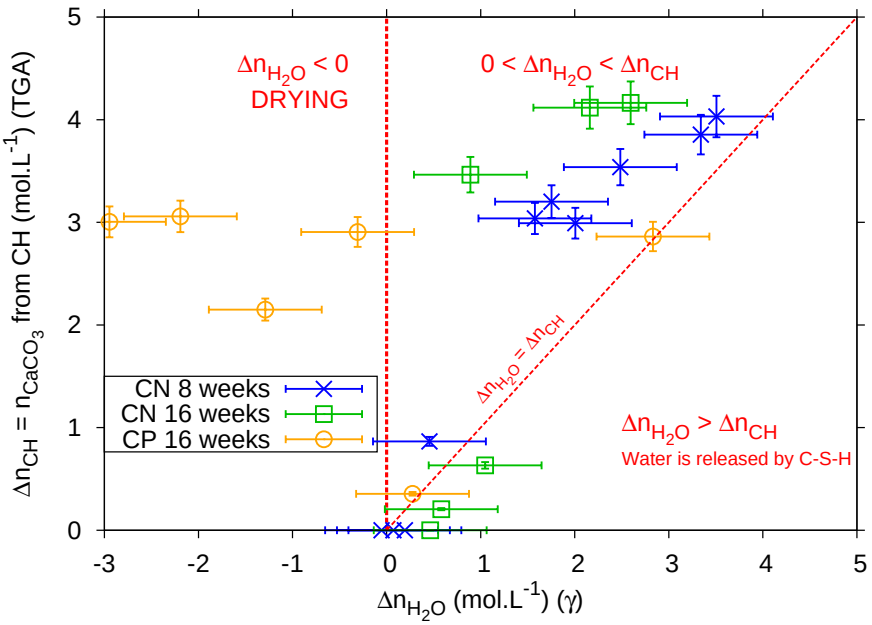

Figure 24: Molar content of water released along the profile (GRAM) after 56 and 112 days of carbonation has been extracted, and is linked to the carbonated amount of CH determined by TGA.

List of Tables

Bogue's phase	(%)
C_3S	59
C_2S	19
C_3A	2
C_4AF	14
gypsum	5

Table 1: Bogue's composition of the studied cement (CEM I 52,5 N CE PM-ES CP2 NF).

Characteristics	Units	CN	CP	Mortar
Porosity (MIP)	[%]	19.2 ± 0.7	31.0 ± 2.1	12.0 ± 1.3
Porosity (water)	[%]	42.4 ± 0.8	50.3 ± 1.8	20.1 ± 2.5
Degree of hydration (mod.)	[-]	0.80	0.92	-
Degree of hydration (TGA)	[-]	0.86 ± 0.02	0.84 ± 0.04	0.97 ± 0.04
CH content (TGA)	[mol.L^{-1}]	4.46 ± 0.12	3.69 ± 0.16	0.94 ± 0.05
C-S-H content (model)	[mol.L^{-1}]	4.59	3.75	-

Table 2: Main physical and chemical characteristics of the studied cement pastes CN and CP after a sealed curing period of 6 months. The assessment of CH content and degree of hydration are performed by TGA. Porosity is measured either by MIP or by hydrostatic weighing [56]. A simple hydration model based on Powers' theory [81] is used to assess the degree of hydration, as well as C-S-H content. The stoichiometry of C-S-H is fixed here at $C_{1.7}S_1H_{1.5}$.